Turbulent statistical characteristics associated to the north wind phenomenon in southern Brazil with application to turbulent diffusion

Gervasio Annes Degrazia

2014

Available online at www.sciencedirect.com
ScienceDirect
Physica A 387 (2008) 4376–4386
PHYSICA A
www.elsevier.com/locate/physa

Turbulent statistical characteristics associated to the north wind phenomenon in southern Brazil with application to turbulent diffusion

Maria Cristina Andres Arbage, Gervásio Annes Degrazia*, Guilherme Sausen Welter, Débora Regina Roberti, Otávio Costa Acevedo, Osvaldo Luiz Leal de Moraes, Simone Teleginski Ferraz, Andréa Ucker Timm, Virnei Silva Moreira

Abstract

A parameterization for the transport processes in a shear driven planetary boundary layer (PBL) has been established employing turbulent statistical quantities measured during the north wind phenomenon in southern Brazil. Therefore, observed one-dimensional turbulent energy spectra are compared with a spectral model based on the Kolmogorov arguments. The good agreement obtained from this comparison leads to well defined formulations for the turbulent velocity variance, local decorrelation time scale and eddy diffusivity. Furthermore, for vertical regions in which the wind shear forcing is relevant, the eddy diffusivity derived from the north wind data presents a similar profile to those obtained from the non-extensive statistical mechanics theory. Finally, a validation for the present parameterization has been accomplished, using a Lagrangian stochastic dispersion model. The Prairie Grass data set, which presents high mean wind speed, is simulated. The analysis developed in this study shows that the turbulence parameterization constructed from wind data for north wind flow cases is able to describe the diffusion in a high wind speed, shear-dominated PBL.

Keywords: Shear driven turbulence; Turbulent parameterization; Lagrangian stochastic dispersion model

1. Introduction

Frequently, in a regional scale at the center of Rio Grande do Sul state (southern Brazil), a phenomenon known as north wind flow (NWF) occurs. It is characterized by intense warm winds from the north, presenting low relative humidity, associated to meteorological frontal systems. During this phenomenon, occurring most frequently in winter months (June, July and August), a system of low pressure is observed in the atmospheric circulation with low levels (1000 mb) to the South of the South America and high pressure in the extratropical Atlantic. The relative humidity is lower than the average with anomalies around −10% in the Rio Grande do Sul, and winds from the north more

* Corresponding author. Tel.: +55 5532208616; fax: +55 5532208616.
E-mail address: degrazia@ccne.ufsm.br (G.A. Degrazia).

0378-4371/$ - see front matter
doi:10.1016/j.physa.2008.02.068

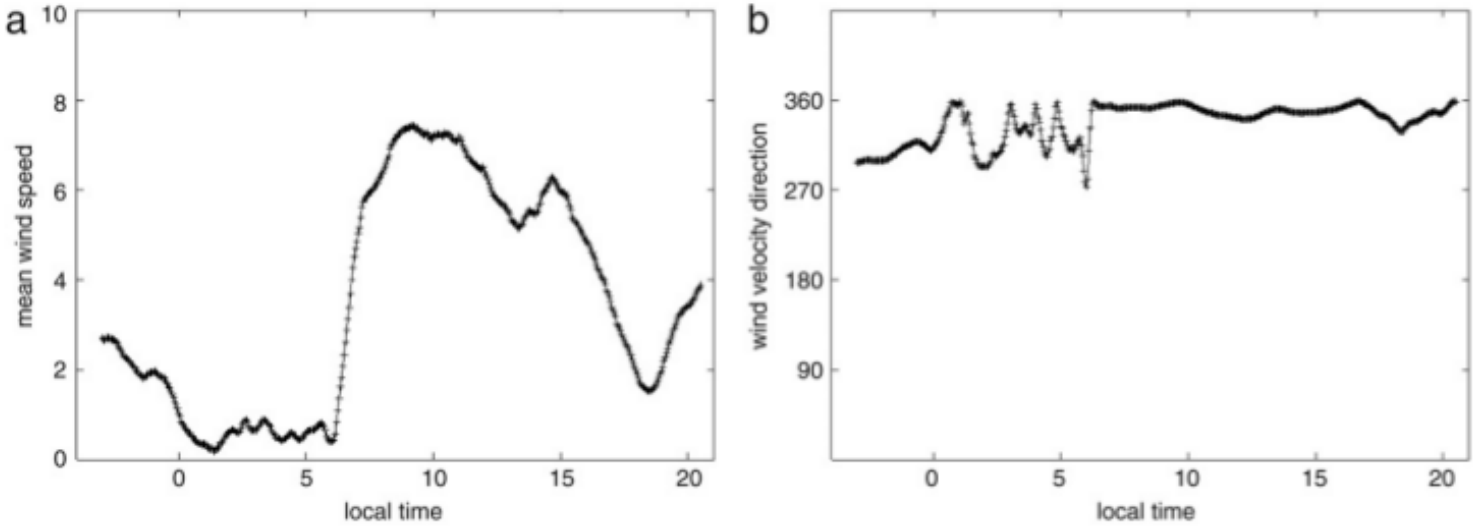

Fig. 1. Characteristic values of the mean wind speed in m s^{-1} for a North Wind case; (b) characteristic wind direction in degrees for a North Wind case.

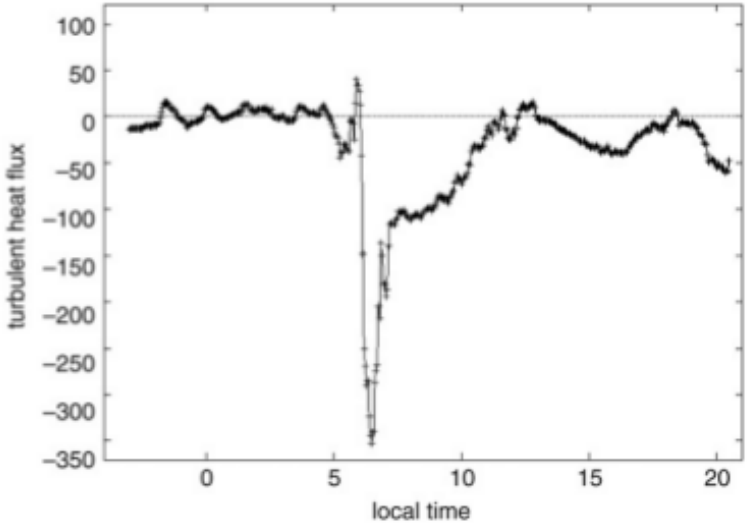

Fig. 2. Turbulent heat flux in W m^{-2}.

intense than the average in the same region. The wind anomaly shows that this north flow is accelerated by the action of the local topography, which reinforces its magnitude, transporting drier air from northern regions. Figs. 1a, b show, respectively, the magnitude (ms^{-1}) and direction (degrees) of the NWF for a typical day in Paraíso do Sul city (center of Rio Grande do Sul). It can be seen that the magnitude of the wind at certain moment changes abruptly from low to high values, characterizing the presence of this particular flow. Furthermore, observation of Fig. 1b confirms the dominant north direction associated with this flow. For the same case exhibited in Fig. 1a and 1b, Fig. 2 shows the turbulent sensible heat flux ($W\,m^{-2}$). From this figure it can be seen that there is a negative sensible heat flux occurring near noon. This anomalous behavior associated with the heat flux shows that dry and warm air has been transported by this intense NWF and has created a situation, in which the near surface temperature is higher than those in the soil. This sensible heat flux pattern identifies a stable boundary layer, which usually occurs at night. However, in the presence of the NWF, an unexpected situation arises, during which a negative turbulent heat flux is observed at daytime.

The aim of this study is to use Taylor's statistical diffusion theory together with a model for the turbulent spectra in a shear driven planetary boundary layer (PBL), in order to evaluate the turbulent statistical parameters associated to the NWF occurring in the central region of the Rio Grande do Sul state. Relevant micrometeorological quantities, such as the friction velocity, turbulence dissipation rate and the spectral peak frequencies were measured and employed to calculate the turbulent velocity variances and the decorrelation time scales for the north wind occurrences. These turbulent parameters derived from the north wind were introduced into a Lagrangian stochastic dispersion model to

2. Experimental micrometeorological data associated to the NWF events

In this section micrometeorological statistical parameters associated to the NWF phenomenon are obtained and analyzed. Data were collected at a continuously measuring site, at Paraíso do Sul (S 29°44′39.6″, W 53°09′59.8″), in southern Brazil. The micrometeorological tower is a part of CT-HIDRO project, a Brazilian-wide study with the purpose of describing the surface conditions for distinct ecosystems in the country. The tower is located at a flat site, with a hill to the north. Turbulence is measured at the 10 m height by a Campbell 3-D sonic anemometer employing a sample rate of 16 Hz. Other measurements include the radiative energy budget components, soil temperature and moisture content at five levels, as well as slow response wind, temperature, relative humidity and pressure.

The data used in this study consist of 7 NWF cases from May, July and August, 2004. Each case has a duration period of approximately 4 days. Evolutions of the micrometeorological parameters that need the estimation of turbulence statistics were determined using 30 min data windows for the mean removal [1]. The windows are centered at a given data point which advances with 3 min time steps for each series. Before the analyses the individual wind vectors were rotated into the mean wind direction in such a way that $\overline{v} = \overline{w} = 0$. Then, the mean values of wind speed and temperature, surface layer turbulent statistics (u_{*0}, $\overline{w'\theta'}$, L) and standard deviations of the turbulent velocities ($\sigma_i (i = u, v, w)$) were calculated, where u_{*0} is the surface friction velocity, $\overline{w'\theta'}$ is the surface sensible turbulent heat flux and L is the Obukhov length scale. A data quality analysis was applied to detect any spikes, kinks or missing portions in the data.

For characterizing the surface layer structure, turbulent fluxes of heat and momentum were estimated using the eddy correlation technique. The scaling of velocity (surface friction velocity) has been evaluated, at a height of 10 m, from the expression

$$u_{*0} = (\overline{w'u'}^2 + \overline{w'v'}^2)^{1/4} \tag{1}$$

where $\overline{w'u'}$ and $\overline{w'v'}$ are the surface turbulent momentum fluxes in the direction of the u and v components of the wind vector velocity, respectively. Another important surface turbulent parameter is the Obukhov length scale, which was obtained for each test run using

$$L = -\frac{\rho c_p u_{*0}^3}{\kappa (g/T_0)\overline{w'\theta'}} \tag{2}$$

Table 1

Mean quantities (U, T) and the turbulent statistical parameter (u_{*0}, $\overline{w'\theta'}$, L) for the 7 NWF cases

U (m s^{-1})	T (°C)	u_{*0} (m s^{-1})	$\overline{w'\theta'}$ (W m^{-2})	L (m)
7.24	24	0.61	−64.09	197.25

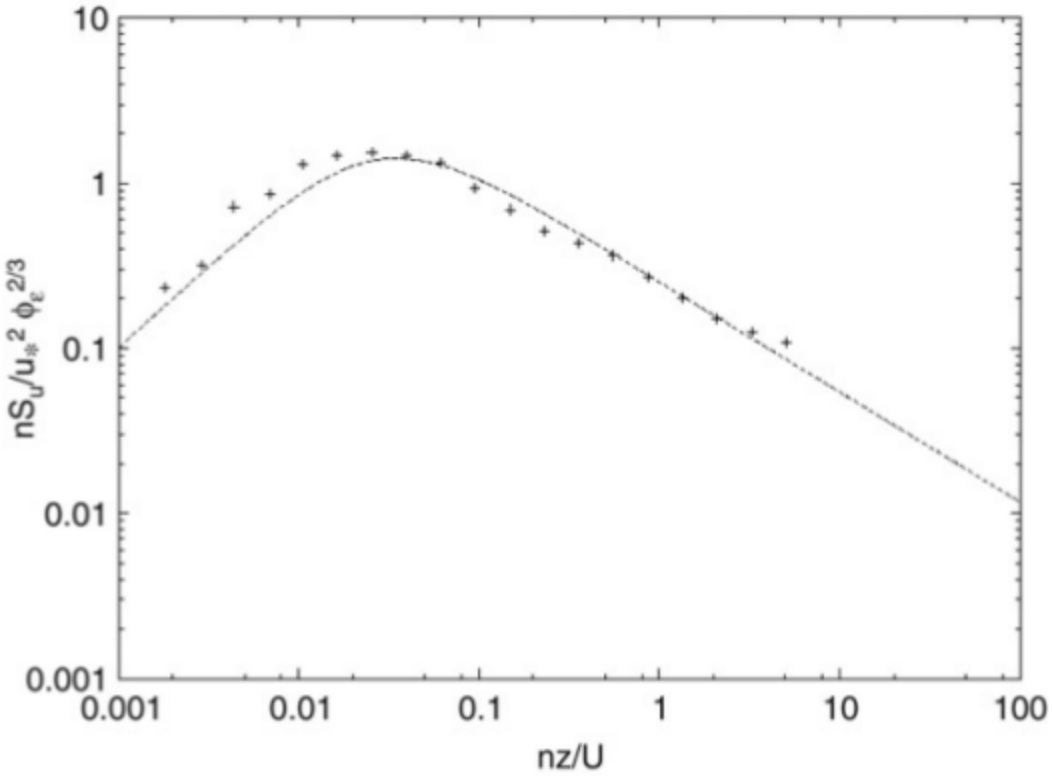
10
1
0.1
0.01
0.001
0.001
0.01
0.1
1
10
100
nz/U
$nS_u/u_*^2\,\phi_\varepsilon^{2/3}$

The spectra were computed using the Fast-Fourier technique and following the steps suggested in Stull [3]. The spectral estimates are block-averaged over 22 non-overlapping frequency bands [4]. The u (longitudinal), v (lateral) and w (vertical) spectra were normalized by $u_{*0}^2 \phi_\varepsilon^{2/3}$ (ϕ_ε is the dimensionless dissipation rate of turbulent kinetic energy). This procedure to normalize the spectral curves has been used in the literature [2,5]. The dimensionless dissipation rate is defined as

$$\phi_\varepsilon = \frac{\kappa z \varepsilon}{u_{*0}^3} \tag{3}$$

where ε is the mean turbulent kinetic energy dissipation per unit time per unit mass of fluid, with the order of magnitude of ε determined only by those quantities that characterize the energy-containing eddies.

Following this framework for setting spectral models and the observed turbulent energy spectra in the surface layer [6], when neutral spectra are plotted against the dimensionless frequency $f = nz/U$ (n being the cyclic frequency, U be mean wind speed and z the observation height) on a log–log scale, they are characterized by a low-frequency slope of $+1$, and by a high-frequency slope of $-2/3$ ($f^{-2/3}$ Kolmogorov's law for the inertial subrange).

Figs. 3–5 present, respectively, the normalized turbulent spectra for the u, v, w velocity components. In these figures, crosses represent the observed spectra while the continuous lines are obtained from the following expression derived by Degrazia et al. [7] and that represents a model to describe measured turbulent spectra in a shear driven PBL

$$\frac{nS_i}{u_*^2} = \frac{1.5c_i\phi_\varepsilon^{2/3} f}{\left(1 + \frac{1.5f^{5/3}}{[(f_m)_i]^{5/3}}\right)[(f_m)_i]^{5/3}} \tag{4}$$

where $i = u, v, w$, $u_*^2 = u_{*0}^2 (1 - z/h)^{1.7}$ is the local friction velocity for a neutral PBL [7], $(f_m)_i$ is the non-dimensional frequency of the neutral spectral peak and $c_i = \alpha_i \alpha_u (2\pi\kappa)^{-2/3}$, $\alpha_u = 0.5 \pm 0.05$, and $\alpha_i = 1, 4/3, 4/3$ for u, v and w components, respectively [8,9].

It can be seen that all the spectra at the high-frequency follow approximately Kolmogorov's $-2/3$ slope. Furthermore, the model as given by (4) fits well the observed spectra in the frequency range containing the most energy.

The peak frequencies $(f_m)_u$, $(f_m)_v$ and $(f_m)_w$ are important for studies of scalar turbulent transport in the PBL and merit close analysis. For the neutral case, these peak frequencies describing the spatial and temporal characteristic

of the energy-containing eddies, are expressed by the following formulation [3,7,10–12]

$$(f_m)_i = (f_m)_{0i}\left(1 + 0.03a_i\frac{f_c z}{(u_*)_0}\right) \tag{5}$$

where $(f_m)_{0i}$ is the frequency of the spectral peak in the surface, $f_c = 10^{-4}$ s^{-1} is the Coriolis parameter, with $a_u = 500$, $a_v = 1094$, and $a_w = 3889$. For the NWF events, measured in this study, the peak frequencies in the surface occurred in the range $0.015 < (f_m)_{0u} < 0.060$; $0.085 < (f_m)_{0v} < 0.30$; $0.19 < (f_m)_{0w} < 0.70$ with mean values of $(f_m)_{0u} = 0.040$, $(f_m)_{0v} = 0.10$ and $(f_m)_{0w} = 0.33$. These estimated values of the spectral peak frequencies are in fair agreement with the values obtained from the experimental data measured in Kansas and Minnesota experiments [6].

The simplest measure of turbulent velocity fluctuation levels are the variances or mean-square fluctuations σ_u^2, σ_v^2 and σ_w^2. These parameters represent quantities that allow the turbulence intensity estimation. Therefore, they are important in determining the longitudinal, lateral and vertical dispersion of contaminants. From the experimental spectral data, the following values for the turbulent velocity variances were calculated: $\sigma_u = 2.67u_{*0}$, $\sigma_v = 1.95u_{*0}$ and $\sigma_w = 1.39u_{*0}$. Results for these quantities published in Panofsky and Dutton [13], and applied in situations of stability in which mechanical purely turbulence prevails, suggest the following values: $\sigma_u = 2.40u_{*0}$, $\sigma_v = 1.90u_{*0}$ and $\sigma_w = 1.30u_{*0}$. This comparison shows that the turbulent velocity variances, measured during the NWF phenomenon, are in good agreement with the values found in the literature when mechanical turbulence is dominant.

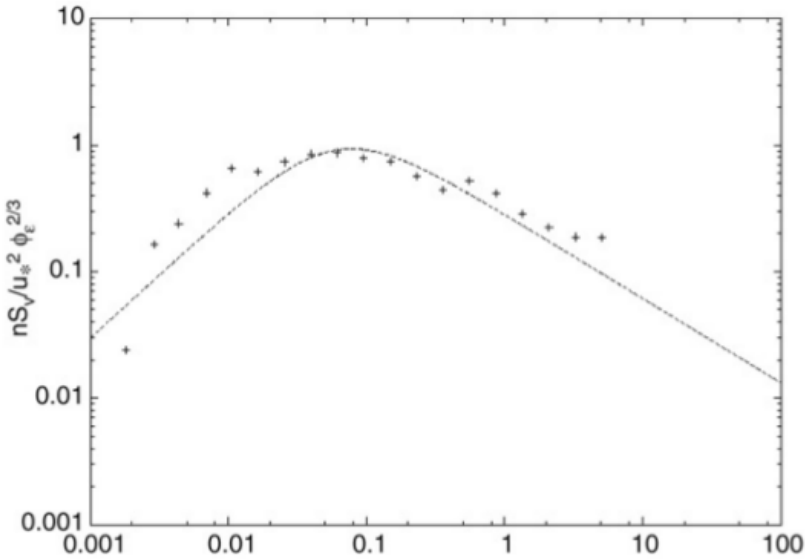

Fig. 4. Spectrum of the lateral turbulent velocity of the NWF normalized by the mechanical rate of TKE dissipation and for the friction velocity. The dashed line represents the spectral model as given by Eq. (4) and the crosses represent the observed spectral data.

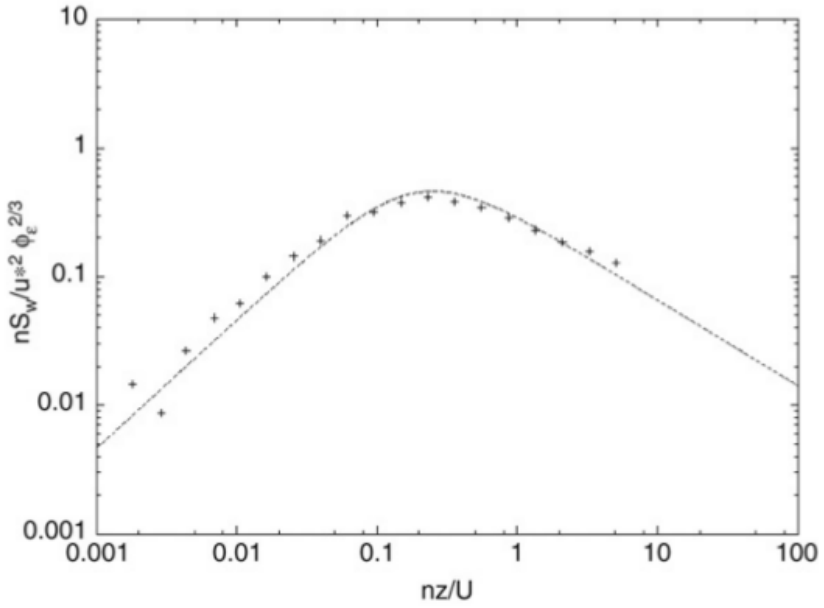

Fig. 5. Spectrum of the vertical turbulent velocity of the NWF normalized by the mechanical rate of TKE dissipation and for the friction velocity. The dashed line represents the spectral model as given by Eq. (4) and the crosses represent the observed spectral data.

It is important to note that to calculate the above velocity variances from the observed turbulent spectra, values of the dimensionless dissipation rate, ϕ_ε, are necessary. Thusly, the dissipation rate of turbulent kinetic energy for each test run has been obtained from the inertial subrange of the one-dimensional spectra of vertical velocity fluctuations using Kolmogorov's law [14].

At neutral stability it is expected that ϕ_ε approaches unity due to the balance between shear production and viscous dissipation of turbulence in the absence of any buoyant production and transport. Our result $\phi_\varepsilon(z/L \to 0) = 1.1$ is in good agreement with Kansas results [15] as well with the theoretical predictions [9].

4. Determination of the Lagrangian decorrelation time scale for the NWF phenomenon

Based on the model for the spectra of turbulent kinetic energy and Taylor statistical diffusion theory [16] derived a formulation for the Lagrangian decorrelation time scales and wind velocity variances for fully developed turbulence.

For a non-homogeneous turbulence these decorrelation time scales can be expressed as:

$$T_{L_i} = \frac{\beta_i F_i^E (n \to 0)}{4} \tag{6}$$

where $\beta_i = 0.55\frac{U}{\sigma_i}$ [17–20] is defined as the ratio of the Lagrangian to the Eulerian decorrelation time scale and $F_i^E (n \to 0) = \frac{S_i (n \to 0)}{\sigma_i^2}$ represents the spectra in which the high frequencies were filtered.

On the other hand, analytical integration of Eq. (4) over the whole frequency domain leads to the following turbulent velocity variance

$$\sigma_i^2 = \frac{2.32 c_i \phi_\varepsilon^{2/3} u_*^2}{(f_m)_i^{2/3}} \tag{7}$$

that is employed to normalize the spectrum. The normalized spectrum can now be written as follows:

$$F_i^E\,(n \to 0) = \frac{S_i(n \to 0)}{\sigma_i^2} = \frac{0.64 z}{(f_m)_i U}. \tag{8}$$

In neutral conditions, the local decorrelation time scales can be derived from Eqs. (6) and (8) as

$$T_{L_i} = 0.088 \frac{z}{\sigma_i (f_m)_i}. \tag{9}$$

Therefore, Eqs. (7) and (9) can be used in a Lagrangian stochastic dispersion model to reproduce observed concentrations of contaminants released in a turbulent field generated by NWF.

Therefore, Eqs. (7) and (9) can be used in a Lagrangian stochastic dispersion model to reproduce observed concentrations of contaminants released in a turbulent field generated by NWF.

As a test for the present model we calculate from Eq. (7) the turbulent velocity variances for the NWF. Therefore, we substitute in Eq. (7) $(f_m)_{0u} = 0.04$, $(f_m)_{0v} = 0.10$, $(f_m)_{0w} = 0.33$ and $\phi_\varepsilon(z/L \to 0) = 1.1$, to obtain, respectively $\sigma_u = 2.46u_*$, $\sigma_v = 2.0u_*$ and $\sigma_w = 1.38u_*$. Comparing the values of the turbulent velocity standard deviations obtained from Eq. (7) employing the observed turbulent parameters for the NWF cases with those extracted from the experimental spectral curves (Section 3), it can be seen that the measured turbulent velocity standard deviations at the surface can be well reproduced by the Eq. (7) derived from the spectral model given by Eq. (4). Therefore, based on this analysis, the typical velocities, length scales and time scales associated with the turbulent field generated by the NWF can be obtained using the formulations given by Eqs. (4), (7) and (9). Furthermore, from Eqs. (5), (7) and (9), using $(f_m)_{0w} = 0.33$, $u_*^2 = u_{*0}^2(1 - z/h)^{1.7}$ and $\phi_\varepsilon(z/L \to 0) = 1.1$, we can derive a vertical eddy diffusivity for a shear-dominated PBL. This eddy diffusivity describes the magnitude of the turbulent transport and can be written as

$$\frac{K_z}{u_{*0}h} \cong \frac{0.4z/h(1 - z/h)^{0.85}}{\left[1 + 15\frac{f_c z}{u_{*0}}\right]^{4/3}} \tag{10}$$

where h is the depth of the neutral PBL which is given by [13,21]

$$h = \frac{0.2u_{*0}}{|f_c|}. \tag{11}$$

Therefore, the substitution of Eq. (11) into Eq. (10) results in

$$\frac{K_z}{u_{*0}h} \cong \frac{0.4z/h(1-z/h)^{0.85}}{[1+3.0z/h]^{4/3}}. \tag{12}$$

Fig. 6 shows the vertical eddy diffusivity profile calculated from Eq. (12). At this point, it is important to note that Eq. (12) provides a K_z profile in lower and central regions of the neutral PBL with the same structure as proposed by Campos Velho et al. [22] which is based on non-extensive statistical mechanics [23]. Futhermore, the neutral eddy diffusivity provided by Eq. (12) presents a profile and magnitudes that agree with the formulation proposed by Garrat [21].

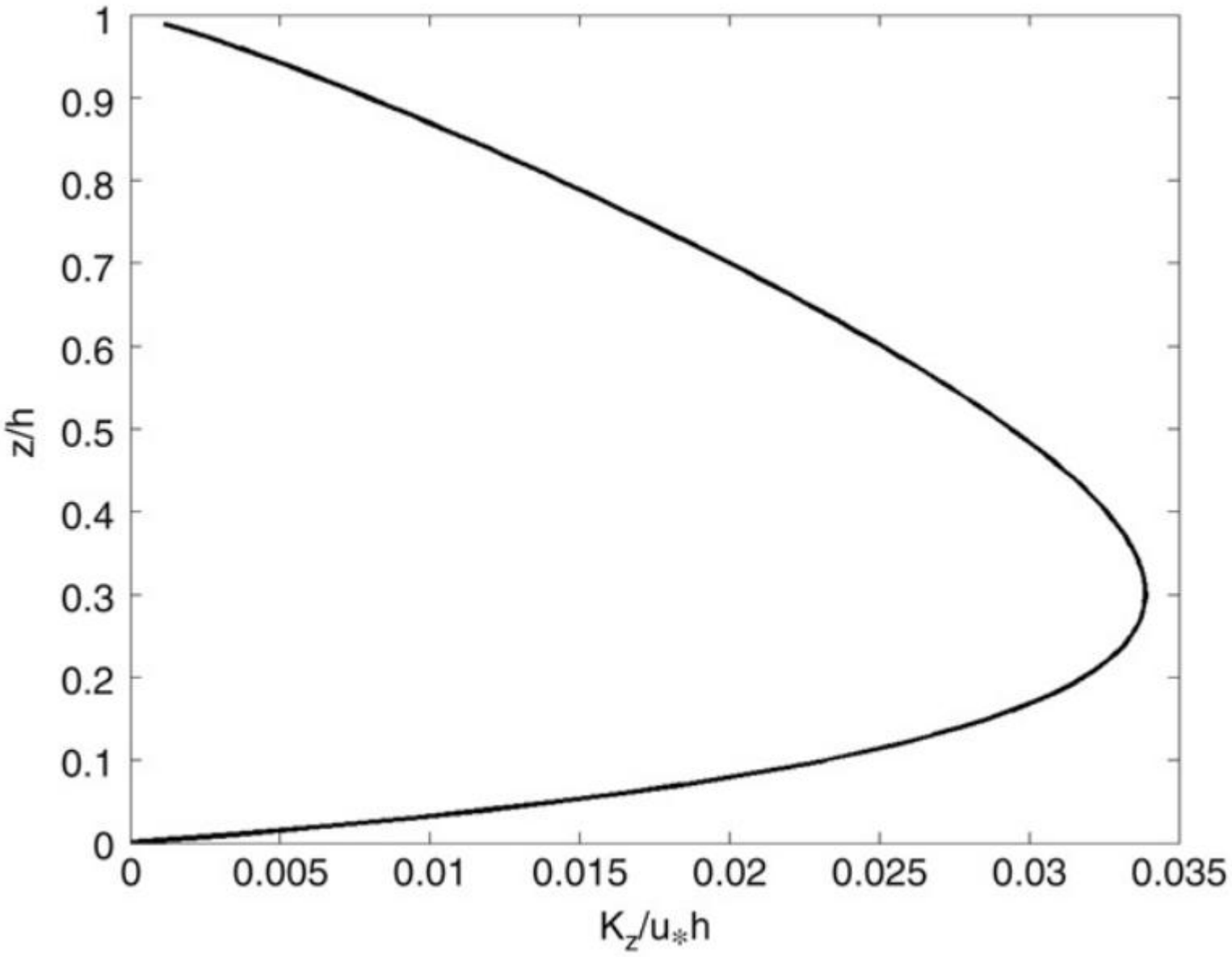
1
0.9
0.8
0.7
0.6
0.5
0.4
0.3
0.2
0.1
0
z/h
0
0.005
0.01
0.015
0.02
0.025
0.03
0.035
K_z/u_*h

5. Test of the proposed parameterization with the Prairie Grass tracer experiment

In this section, we test the values of ϕ_ε and $(f_m)_{0i}$ measured from the NWF events in an application to air contaminant dispersion. Therefore, a Lagrangian stochastic dispersion model employing the measured values of $(f_m)_{0u} = 0.04$, $(f_m)_{0v} = 0.10$, $(f_m)_{0w} = 0.33$ and $\phi_\varepsilon = 1.1$ in Eqs. (7) and (9) has been utilized to simulate the measured concentration data. Lagrangian stochastic particle models are powerful computational tools for the investigation of the atmospheric dispersion process [24]. In these models, the fluid particle displacements are produced by stochastic velocities and the movement evolution of a particle can be considered a Markov process [25] in which past and future are statistically independent when the present is known. This method is based on Langevin equation, which is derived from the hypothesis that the velocity is given by the combination between a deterministic term and a stochastic term [26]. Each fluid particle moves taking into account the transport due to the mean wind velocity and the turbulent fluctuations of the wind velocity components. From the spatial distribution of the particles it is possible to determine the contaminant concentrations. The implementation of the Lagrangian stochastic dispersion model permits the taking into account of complex situations such as the presence of different topographies [27], low wind velocities [28] and spatial and temporal variations of the meteorological fields. These models can simulate sources of different forms and dimensions, as well as continuous, variable in time and instantaneous sources. For a better understanding of these models we suggest the important review paper by Ref. [29]. This work presents historical and basic description about Lagrangian stochastic dispersion models in the PBL.

The actual atmospheric conditions associated with the NWF cases are characterized by intense mean wind speeds and, consequently, for these situations, wind shear forces generate a dominant mechanical turbulence. Therefore, one of the main peculiarities of the present turbulent parameterization (obtained from the NWF cases) is to be able to deal with turbulent dispersion in neutral situations. From these arguments we decided to simulate the classical Prairie Grass tracer dispersion experiments [30] that occurred under high mean wind speed conditions.

The Prairie Grass experiment was performed in O'Neill, Nebraska, in 1956 and it is described in detail by Ref. [30]. The contaminant (SO_2) was emitted without buoyancy at a height of 0.5 m and it was measured by samplers at a height

of 1.5 m at five downwind distances (50, 100, 200, 400, 800 m). The Prairie Grass site was flat with a roughness length of 0.6 cm. From the Prairie Grass runs we select thirteen cases in which the mean wind speed was greater than 6.0 m s^{-1} with values of $(u_*)_0 \geqslant 0.4$ m s^{-1}. Table 2 provides the values of the micrometeorological parameters for the selected Prairie Grass runs. The values of U and u_{*0} expressed in Table 2, represent characteristic values of a neutral PBL [21].

The Prairie Grass tracer dispersion was simulated by the Lagrangian particle model LAMBDA [31,32]. For a detailed presentation and discussion of LAMBDA we refer to the quoted papers. The actual version of the LAMBDA dispersion model is based on the generalized Langevin equation [33], whose coefficients are obtained by solving the Fokker–Planck equation, and satisfies the well-mixed condition. It can use, as input, higher-order moments of the atmospheric probability density function (PDF) of wind velocity. In the present application, LAMBDA used a Gaussian PDF on the horizontal plane and a Gram-Chalier PDF, truncated to the fourth order, in the vertical.

All the available data (see Table 2) were used to create an input file for the simulations. The profiles of wind standard deviations (σ_i) and the local decorrelation time scales (T_{Li}), which were used in the LAMBDA dispersion model, were calculated according to Eqs. (7) and (9), with $(f_m)_i$ given by Eq. (5) and considering a neutral PBL $u_*^2 = u_{*0}^2 (1 - z/h)^{1.7}$ [7,34].

LAMBDA simulation results are presented in Table 2. The model performances are shown in Table 3 and Fig. 7. Table 3 exhibits the result of the statistical analysis made with observed and predicted values of ground-level cross-wind integrated concentration (C_y). Additionally, Table 3 presents a comparison between the turbulent parameterization derived from the NWF cases (present parameterization) with the one from Hanna [35] for the neutral condition. This last parameterization was chosen for the comparison because it is well known and widely used in the literature. The statistical indices in Table 3 are suggested by Hanna [36]:

Table 2
Meteorological parameters and ground-level cross-wind-integrated concentration (C_y) measured during the Prairie Grass experiment

Run	h (m)	u_{*0} (m s^{-1})	U_{10m} (m s^{-1})	Q (gs^{-1})	50 m (gm^{-2})	100 m (gm^{-2})	200 m (gm^{-2})	400 m (gm^{-2})	800 m (gm^{-2})
5	780	0.40	7.0	78	3.30	1.80	0.81	0.29	0.092
					3.40	1.82	0.84	0.39	0.19
9	550	0.48	8.4	92	3.70	2.20	1.00	0.41	0.13
					3.33	1.79	0.88	0.40	0.18
19	650	0.41	7.2	102	4.50	2.20	0.86	0.27	0.058
					4.24	2.19	1.07	0.50	0.28
20	710	0.63	11.3	102	3.40	1.80	0.85	0.34	0.13
					2.40	1.28	0.72	0.34	0.17
26	900	0.45	7.8	98	3.90	2.20	1.04	0.39	0.127
					3.82	2.04	1.09	0.51	0.23
27	1280	0.44	7.6	99	4.30	2.30	1.16	0.46	0.176
					3.85	2.13	1.00	0.50	0.25
30	1560	0.48	8.5	98	4.20	2.30	1.11	0.40	0.10
					3.57	1.93	0.90	0.41	0.24
43	600	0.40	6.1	99	5.00	2.40	1.09	0.37	0.12
					4.81	2.30	1.22	0.62	0.29
44	1450	0.42	7.2	101	4.50	2.30	1.09	0.43	0.14
					4.17	2.24	1.10	0.51	0.27
49	550	0.47	8.0	102	4.30	2.40	1.16	0.45	0.15
					3.68	1.86	1.03	0.48	0.25
50	750	0.46	8.0	103	4.20	2.30	0.91	0.39	0.11
					3.68	1.90	0.96	0.51	0.27
51	1880	0.47	8.0	102	4.70	2.40	1.00	0.38	0.084
					3.50	2.01	0.96	0.47	0.27
61	450	0.53	9.3	102	3.50	2.10	1.14	0.53	0.20
					3.10	1.67	0.84	0.45	0.21

$$NMSE = \overline{(C_o - C_p)^2}/(\overline{C_o} \cdot \overline{C_p}) \quad \text{(Normalized Mean Square Error)}$$

$$FB = (\overline{C_o} - \overline{C_p})/(0.5(\overline{C_o} + \overline{C_p})) \quad \text{(Fractional Bias)}$$

$$FS = 2\left(\sigma_o - \sigma_p\right) / \left(\sigma_o + \sigma_p\right) \quad \text{(Fractional Standard Deviation)}$$

$$R = \overline{(C_o - \overline{C_o})(C_p - \overline{C_p})}/\sigma_o\sigma_p \quad \text{(Correlation Coefficient)}$$

$$FA2 = 0.5 \leq C_o/C_p \leq 2 \quad \text{(Factor 2)}$$

Table 3
Statistical evaluation indices considering Hanna's model for the Prairie Grass experiment

	NMSE	COR	FA2	FB	FS
NWF	0.04	0.99	0.92	0.08	0.14
Hanna (1982)	0.40	0.95	0.78	0.41	0.39

6. Conclusions

In this study, we employed Taylor's statistical diffusion theory, a model that describes observed turbulent spectra and a Lagrangian stochastic particle model, to investigate turbulent statistical characteristics and diffusive properties associated with the north wind phenomenon. This NWF consists of a warm air flow that occurs in a regional scale in the winter period in southern Brazil. It is characterized by high mean wind magnitudes and generates a shear-dominated atmospheric boundary layer. Wind turbulent data for seven NWF cases were utilized to generate one-dimensional turbulent energy spectra, experimental values of the surface spectral peak frequencies, and velocity variances. The values of these observed variances and spectral peak frequencies exhibit a good agreement with the

results of literature. Thusly, the comparison indicates that the transport process in the PBL generated by the NWF is dominated by mechanical turbulence.

The peak frequencies and velocity variances describe the temporal and spatial scales of the energy-containing eddies and therefore they are important for studies of turbulent transport in the PBL. Thusly, to obtain a turbulence parameterization, the NWF energy spectra were compared with fitting curves obtained from a spectral model based on Kolmogorov hypothesis for a fully developed turbulence (Eq. (4)). The comparison shows that, in the turbulent motion frequency range, the observed energy spectra are well represented by the curves generated by the spectral model. As a consequence of this result, formulations for the velocity variances (Eq. (7)), and local decorrelation time scales (Eq. (9)), expressed in terms of the observed statistical variables associated with the NWF cases (ϕ_ε, $(f_m)_{0i}$), become well defined and can be used as physical turbulent parameters in dispersion models. Therefore, a vertical turbulent diffusivity has been derived (Eq. (12)) and compared with an eddy diffusivity derived from the non-extensive statistical mechanical concepts that describes turbulent transport generated by mechanical forcing. This comparison shows that both values of eddy diffusivity exhibit a similar profile in vertical regions in which the wind shear force is dominant.

The present turbulent parameterization representing the dispersion condition in a shear dominated PBL occurring during the NWF cases, was evaluated and validated through a comparison with experimental concentration data. Particularly, the results obtained by the Langrangian stochastic particle model LAMBDA, incorporating the parameterization derived from the turbulent statistical characteristics associated to the NWF, agree very well with the experimental concentration data, indicating that the model represents the diffusion process correctly in intense wind speed neutral conditions. It is also possible to verify that the simulated results employing the parameterization derived from the NWF data are better than those obtained by the Hanna's parameterization model.

Considering the statistical evaluation and the arguments discussed above the parameterization for the NWF phenomenon allied to the Lagrangian dispersion model LAMBDA is found to be suitable to simulate the diffusion of passive scalars in a intense wind speed neutral PBL.

2.1 Espectros de velocidade turbulenta unidimensionais na CLP

2.1.a O espectro turbulento na Camada Limite Convectiva (CLC)

A CLC é geralmente caracterizada por uma ascensão turbulenta do fluxo de calor sensível H da superfície ($H>0$). Isto ocorre através de um gradiente negativo gerado pela diferença de temperatura entre a superfície e a camada de ar superior. Para o ar seco, podemos escrever a expressão do fluxo de calor sensível como $H=\rho c_p\left(\overline{w'\theta'}\right)_0$, onde ρ é a densidade do ar, c_p é a capacidade de calor específico a pressão constante do ar seco e $\left(\overline{w'\theta'}\right)_0$ é o fluxo de calor cinemático superficial. Os parâmetros característicos de uma CLC homogênea e estacionária são a velocidade de fricção superficial $(u_*)_0$, o fluxo de empuxo $\frac{g}{\theta}\left(\overline{w'\theta'}\right)_0$ (g é a aceleração da gravidade e $\overline{\theta}$ é a temperatura potencial média), o parâmetro de Coriolis f_c e a altura da camada de mistura z_i, a qual é usualmente definida como a altura até a base de inversão mais baixa (Nieuwstadt, 1980).

Segundo Caughey (1981) e Garrat (1992) a estrutura da CLC (a qual ocorre desde o nascer do sol até o final da tarde), pode ser dividida da seguinte forma:

a) Camada Superficial

Na camada superficial, a turbulência de origem mecânica (gerada pelo cisalhamento do vento) desempenha um papel dominante até regiões verticais caracterizadas por $z \leq |L|$ (z é a altura acima da superfície), onde a teoria de Monin–Obukhov é válida. Nesta camada os perfis médios adimensionais, como espectro e estatísticas integrais dependem do parâmetro z/L. Por outro lado, as componentes turbulentas das velocidades horizontais adimensionais dependem do parâmetro z_i/L. Aqui L é a escala de comprimento de Monin–Obukhov definida como

$$L = -\frac{(u_*)_0^3}{k\frac{g}{\theta}\left(\overline{w'\theta'}\right)_0} \qquad (4)$$

onde $k = 0.4$ é a constante von Karman.

b) Camada de convecção livre

Na Camada de convecção livre, definida no intervalo de $|L| < z < 0.1 z_i$ $(u_*)_0$ não é uma escala de velocidade relevante enquanto z ainda é uma escala importante. De fato $(u_*)_0$ na prática nunca tende à zero, mas a condição de convecção livre local determina a escala para a estrutura turbulenta.

c) Camada de mistura

A camada de mistura compreende a maior parte da CLC, com $0.1<z/z_i<1$. A estrutura da turbulência é insensitiva a z e a $(u_*)_0$. A escala de velocidade característica então será w_* (escala de velocidade convectiva), onde

$$w_* = \left(\frac{g}{\theta} \left(\overline{w'\theta'} \right)_0 z_i \right)^{1/3} \qquad (5)$$

Ao mesmo tempo, a escala de tempo convectiva z_i/w_* na camada de mistura é muito menor que f_c^{-1}, dessa forma, a dependência da estrutura turbulenta de f_c pode ser desprezada. Isto quer dizer que do ponto de vista estatístico a turbulência pode ser descrita em termos dos parâmetros característicos w_* e z_i. Isto é conhecido como a similaridade da CLC (Deardorff, 1972; Willis e Deardorff, 1974).

d) Camada interfacial de entranhamento ou zona de entranhamento

A camada interfacial de entranhamento está compreendida de $0.8\,z_i$ *a* $1.2\,z_i$. Nesta região a estrutura da turbulência pode ser dominada por efeitos de entranhamento, pelas características da capa de inversão e pela atmosfera estável acima. Observações de sondas acústicas revelaram a evidência de uma inversão flutuante, com penetrações de termas convectivas vindas debaixo. As escalas da

camada de mistura não podem assumir um comportamento universal nesta região.

Muitos espectros de velocidade unidimensionais turbulentos na CLP apresentam uma forma simples. No intervalo de freqüências que representa o movimento turbulento, eles podem ser freqüentemente bem representados por uma curva suave com um único máximo (quando plotados como lognS(n) versus logn). Esta afirmação é válida para todas as componentes da velocidade em condições de turbulência dominadas pelo cisalhamento do vento, para o espectro da componente "w" (que é o espectro da velocidade vertical turbulenta) em condições instáveis. Já, para os espectros no caso convectivo as componentes horizontais "u" e "v" (que são os espectros das velocidades longitudinais e laterais) podem ter uma estrutura levemente diferente com a tendência de apresentar dois picos (Panofsky e Dutton, 1984, pág. 196).

Segundo Olesen et al. (1984) a expressão geral para descrever o espectro de velocidade unidimensional na CLP tem a seguinte forma:

$$\frac{n S_i^E(n)}{(u_*)_0^2} = \frac{A f^{\gamma}}{\left(1 + B f^{\alpha}\right)^{\beta}} \qquad (6)$$

Na expressão acima, n é a freqüência em ciclos/segundo ou hertz, $S_i^E(n)$ é o espectro de velocidade unidimensional em função da freqüência, $f = nz/U$ é a freqüência reduzida, U é a componente da velocidade longitudinal média do vento, $A, B, \alpha, \beta \; e \; \gamma$ são constantes, dependendo, portanto, das condições atmosféricas. Espectros que

apresentam essa forma são caracterizados por uma inclinação de baixas freqüências em γ quando plotados no formato log versus log, e por uma inclinação de altas freqüências para $\gamma - \alpha\,\beta$. Os espectros são mais ou menos pontiagudos dependendo dos valores de $\alpha, \beta\ e\ \gamma$, ou seja, $\alpha, \beta\ e\ \gamma$ determinam a forma do espectro. As constantes $A\ e\ B$ não influenciam a forma do espectro, mas somente a sua posição.

Quando construímos um modelo com o formato da expressão (6), somos livres para escolher um certo número de critérios diferentes de modo a determinar os coeficientes desconhecidos envolvidos.

Como uma conseqüência, primeiramente, um modelo espectral deverá ser consistente com a lei do subintervalo inercial de Kolmogorov isto é,

$$E_1(k) = \alpha_1\,\alpha_u\,\varepsilon^{2/3}\,k^{-5/3} \qquad (7)$$

onde $E_1(k)$ é um espectro de velocidade turbulento unidimensional no subintervalo inercial escrito em função do número de onda, ε é a taxa de dissipação média da energia cinética turbulenta, $k = 2\pi n/U$ é o número de onda e $\alpha_u = 0.5 \pm 0.05$ (Champagne et.al, 1977) e α_1 são constantes.

Usando a relação entre o número de onda e a freqüência $k = 2\pi n/U$, a equação (7) pode ser escrita da seguinte forma:

$$\frac{2\pi n}{U}\frac{1}{(u_*)_0^2}E_i\left(\frac{2\pi n}{U}\right)=\alpha_i(0.5\pm0.05)\left(\frac{\varepsilon\kappa z}{(u_*)_0^3}\right)^{2/3}\left(\frac{2\pi nz}{U}\right)^{-2/3}\kappa^{-2/3} \qquad (8)$$

Os termos do lado esquerdo nas expressões (6) e (8) correspondem ao espectro unidimensional normalizado, assim podemos escrever para o subintervalo inercial:

$$\frac{nS_i^E(n)}{(u_*)_0^2}=\alpha_i(0.5\pm0.05)(2\pi\kappa)^{-2/3}\phi_\varepsilon^{2/3}f^{-2/3} \qquad (9)$$

e finalmente

$$\frac{nS_i^E(n)}{(u_*)_0^2}=c_i\phi_\varepsilon^{2/3}f^{-2/3} \qquad (10)$$

onde $\phi_\varepsilon=\varepsilon\kappa z/(u_*)_0^3$ é a taxa de dissipação adimensional na camada superficial e $c_i=\alpha_i(0.5\pm0.05)(2\pi\kappa)^{-2/3}$ com $\alpha_i=1,4/3,4/3$ (condição de isotropia) para as componentes u, v e w respectivamente, implicando que $c_u=0.27$ (para o espectro da componente u) e $c_v=c_w=0.36$ (para os espectros das componentes v e w).

O espectro de velocidade em condições convectivas pode ser obtido da expressão (6) e escrito como

$$\frac{nS_i^E(n)}{w_*^2}=\frac{Af^\gamma}{(1+Bf^\alpha)^\beta}\left(-\frac{\kappa L}{z_i}\right)^{2/3} \qquad (11)$$

onde a relação

$$\frac{w_*^2}{(u_*)_0^2} = \left(\frac{z_i}{-\kappa L} \right)^{2/3}$$

foi usada. Na CLC, o subintervalo inercial para o espectro de velocidade turbulenta pode ser calculado da expressão (10) e representado como

$$\frac{n S_i^E(n)}{w_*^2} = c_i \kappa^{2/3} f^{-2/3} \psi_\varepsilon^{2/3} \left(\frac{z}{z_i} \right)^{2/3} \qquad (12)$$

onde $\psi_\varepsilon = \left(\varepsilon_b z_i / w_*^3 \right)$ é a função de dissipação adimensional associada ao forçante convectivo da turbulência e ε_b é a dissipação devida ao forçante convectivo.

Para grandes freqüências (quando $n \to \infty$), a expressão (11) terá a forma abaixo

$$\frac{n S_i^E(n)}{w_*^2} = \frac{A}{B^\beta} f^{\gamma - \alpha\beta} \left(-\frac{\kappa L}{z_i} \right)^{2/3} \qquad (13)$$

Se o modelo da expressão (11) é consistente com a lei de Kolmogorov, então a comparação entre as expressões (12) e (13) conduz a duas condições: uma se referindo a forma das altas freqüências assimptóticas

$$\gamma - \alpha\,\beta = -\frac{2}{3} \tag{14}$$

e a outra em relação à posição

$$A = c_i\,\kappa^{2/3}\,\psi_\varepsilon^{2/3}\left(\frac{z}{z_i}\right)^{2/3}\left(\frac{z_i}{-\kappa L}\right)^{2/3} B^{\beta} \tag{15}$$

Um outro critério diferente, aparece se exigirmos que a posição observada $\left[\left(f_m\right)_i^c\right]^a$, da freqüência do pico espectral convectivo coincida com o máximo do modelo da expressão (11). Neste caso teremos

$$\frac{d}{df}\left[A f^{\gamma}\left(1 + B f^{\alpha}\right)^{-\beta}\right]\Bigg|_{f=\left[\left(f_m\right)_i^c\right]^a} = 0$$

e agora usando a primeira exigência mencionada anteriormente na expressão (14) podemos obter B como segue

$$B = \frac{1.5\,\gamma}{\left[\left(f_m\right)_i^c\right]^a} \tag{16}$$

E, substituindo as expressões (15) e (16) na forma convectiva da expressão (11) teremos

$$\frac{n S_{lc}^{E}(n)}{w_*^2} = \frac{c_l \kappa^{2/3} \psi_\varepsilon^{2/3} (z/z_i)^{2/3} (1.5\gamma)^{\beta} f^{\gamma}}{\left(1+\frac{1.5\gamma f^{\gamma}}{\left[(f_m^*)_l^c\right]^{\alpha}}\right)^{\beta} \left\{\left[(f_m^*)_l^c\right]^{\alpha}\right\}^{\beta}} \qquad (17)$$

onde agora $\left[(f_m)_l^c\right]^{\alpha}$ é a freqüência reduzida do pico espectral convectivo e $S_{lc}^{E}(n)$ representa o espectro turbulento unidimensional convectivo.

Portanto, é apropriado para o espectro de velocidade Euleriano unidimensional em condições convectivas escolher a forma espectral conforme Olesen et al.. Para este caso com $\gamma=1$, $\alpha=1$ e $\beta=5/3$ em (17), obteremos a seguinte expressão

$$\frac{n S_{lc}^{E}(n)}{w_*^2} = \frac{(1.5)^{2/3} c_l \kappa^{2/3} \psi_\varepsilon^{2/3} (z/z_i)^{2/3} f}{\left[(f_m^*)_l^c\right]^{2/3} \left\{1+1.5\frac{f}{\left[(f_m^*)_l^c\right]}\right\}^{2/3}} \qquad (18)$$

e, finalmente substituindo $\kappa=0.4$ na expressão (18) resulta

$$\frac{n S_{lc}^{E}(n)}{w_*^2} = \frac{1.06 c_l f \left(\psi_\varepsilon \frac{z}{z_i}\right)^{2/3}}{\left[(f_m^*)_l^c\right]^{2/3} \left\{1+1.5\frac{f}{\left[(f_m^*)_l^c\right]}\right\}^{2/3}} \qquad (19)$$

2.1.b O espectro turbulento mecânico (gerado pelo cisalhamento do vento) na CLP

Quando o fluxo turbulento de calor sensível é negativo a única fonte que pode gerar turbulência na CLP é aquela produzida pelo mecanismo do cisalhamento do vento. Na camada limite neutra (CLN) (onde o fluxo de calor superficial é considerado igual a zero), geralmente a energia turbulenta decresce monotonicamente com a altura, e, as escalas de velocidade e comprimento são respectivamente, u_{*_0} e u_{*_0}/f_c. Na CLN superficial (aproximadamente dez por cento da profundidade da CLN), a produção do cisalhamento do vento é grande, aumentando a geração da energia cinética turbulenta. Nesta camada interior, os fluxos turbulentos não diferem muito dos seus valores na superficie (Garrat, 1992).

Em condições de ventos fortes e pouco resfriamento superficial, a turbulência em toda a camada limite estável (CLE) (a qual ocorre na presença de um fluxo de calor superficial negativo), é predominantemente contínua. A turbulência na CLE é muito mais fraca do que aquela que ocorre na CLC já que as forças de empuxo suprimem os vórtices turbulentos, os quais permanecem pequenos e independentes da distância da superficie. Como uma conseqüência, as escalas fundamentais desta turbulência contínua serão descritas em função dos fluxos locais (dependência em z) da tensão de Reynolds e do fluxo de calor turbulento (Niewstadt, 1984; Sorbjan, 1989).

Feitas as considerações para ambos os tipos de CLP dominadas pelo cisalhamento do vento (CLN e CLE com turbulência contínua), o espectro de velocidade unidimensional mecânico pode ser escrito como

$$\frac{n S_i^E(n)}{u_*^2} = \frac{A f^{\gamma}}{\left(1 + B f^{\alpha}\right)^{\beta}} \qquad (20)$$

onde agora u_* é a velocidade de fricção local. Os casos muito estáveis não são descritos pela expressão (20), já que a teoria de Monin–Obukhov não é aplicada nestas condições extremas.

Numa CLP dominada pela turbulência mecânica, o subintervalo inercial para o espectro de velocidade turbulento é dado pela forma da expressão (10)

$$\frac{n S_i^E(n)}{(u_*)^2} = c_i \Phi_\varepsilon^{2/3} f^{-2/3} \qquad (21)$$

onde $\Phi_\varepsilon = \varepsilon_s \kappa z / (u_*)^3$ é a função de dissipação adimensional associada ao forçante mecânico da turbulência e ε_s é a taxa de dissipação mecânica da energia cinética turbulenta.

O comportamento assimptótico da expressão (20) para grandes freqüências terá a seguinte forma

$$\frac{n S_i^E(n)}{u_*^2} = A f^{\gamma - \alpha\beta} B^{\beta} \qquad (22)$$

resultando das expressões (21) e (22) as duas condições

$$\gamma - \alpha\beta = -\frac{2}{3} \qquad (23)$$

$$A = c_i B^{\beta} \Phi_{\varepsilon}^{2/3} \tag{24}$$

Supondo que a posição observada $\left[\left(f_m^* \right)_i^{n+s} \right]^{\alpha}$ da freqüência do pico espectral mecânico esteja concordando com o máximo da expressão (20) teremos

$$B = \frac{1.5\gamma}{\left[\left(f_m^* \right)_i^{n+s} \right]^{\alpha}} \tag{25}$$

Agora, substituindo as expressões (24) e (25) no espectro unidimensional mecânico da expressão (20) resultará:

$$\frac{n S_{is}^{E}(n)}{u_*^2} = \frac{c_i \Phi_{\varepsilon}^{2/3} (1.5\gamma)^{\beta} f^{\gamma}}{\left(1 + \frac{1.5\gamma f^{\alpha}}{\left[\left(f_m^* \right)_i^{n+s} \right]^{\alpha}} \right)^{\beta} \left\{ \left[\left(f_m^* \right)_i^{n+s} \right]^{\alpha} \right\}^{\beta}} \tag{26}$$

onde $\left[\left(f_m^* \right)_i^{n+s} \right]^{\alpha}$ é a freqüência reduzida do pico espectral neutro ou estável e $S_{is}^{E}(n)$ representa o espectro turbulento unidimensional mecânico.

Para o espectro de velocidade Euleriano unidimensional em condições mecânicas expressão (26) escolheremos a forma espectral dada por Olesen et al.. Para este caso $\gamma = 1$, $\alpha = 5/3$ e $\beta = 1$ na expressão (26), e, dessa forma ficaremos com a seguinte expressão

$$\frac{n S_{is}^{E}(n)}{u_{*}^{2}} = \frac{1.5 c_i \Phi_{\varepsilon}^{2/3} f}{\left(1 + \frac{1.5 f^{5/3}}{\left[\left(f_m^*\right)_i^{n+s}\right]^{5/3}}\right)\left\{\left[\left(f_m^*\right)_i^{n+s}\right]^{5/3}\right\}} \qquad (27).$$

$$\frac{M S_i(M)}{\mu_*^2} = \frac{A f^{\gamma}}{(1 + B f^{\alpha})^3} \qquad (1)$$

$$f = \frac{MZ}{U} \quad ; \quad K = \frac{2\pi M}{U}$$

subintervalo inercial

$$E_i(K) = \alpha_i \alpha_\mu \varepsilon^{2/3} K^{-5/3}$$

$$\frac{2\pi M}{U} \quad \frac{1}{\mu_*^2} \quad E_i\left(\frac{2\pi M}{U}\right) = \alpha_i (0.5 \pm 0.05) \left(\frac{\varepsilon K Z}{\mu_*^3}\right)^{2/3}$$

$$\times \left(\frac{2\pi M Z}{U}\right)^{-2/3} K^{-2/3}$$

$$C_i = \alpha_i (0.5 \pm 0.05) (2\pi K)^{-2/3}$$

$$\frac{M S_i(M)}{\mu_*^2} = C_i \left[\frac{\varepsilon K Z}{(\mu_*)^3}\right]^{2/3} f^{-2/3}$$

com $\Phi_\varepsilon = \frac{\varepsilon k z}{(\mu_*)^3}$

$$\frac{M S_i(M)}{\mu_*^2} = C_i \, \Phi_\varepsilon^{2/3} \, f^{-2/3} \qquad (2)$$

No limite quando $f \to \infty$

(1) pode ser escrita como

$$\frac{M S_i(M)}{\mu_*^2} = \frac{A}{B^3} f^{\gamma - \alpha\beta}$$

Se o modelo ① é consistente com a lei de Kolmogorov para o subintervalo inercial resulta:

$$\gamma - \alpha\beta = -\frac{2}{3} \quad ③ \quad e$$

$$\frac{A}{B^3} = C_i \, \bar{\Phi}_\varepsilon^{2/3} \qquad (4)$$

Um outro critério diferente pode ser derivado, q do forçamos que a posição observada da freqüência do pico espectral $(f_m)_i$ coincida com o máximo do modelo

$$\frac{d}{df}\left[A f^{\gamma} (1 + B f^{\alpha})^{-3} \bar{I} \right]_{f=f_m} = 0$$

$$\gamma A f^{\gamma-1} (1+Bf^{\alpha})^{-3} - 3A f^{\gamma} (1+Bf^{\alpha})^{-3-1} \alpha B f^{\alpha-1} = 0$$

$$\gamma + \gamma B f_m^{\alpha} = \alpha 3 B f_m^{\alpha}$$

$$\gamma + (\gamma - \alpha 3) B f_m^{\alpha} = 0$$

de (3), resulta

$$\gamma - \frac{\alpha}{3} B f_m^{\alpha} = 0$$

e

$$B = \frac{1.5\,\gamma^e}{(fm)^\alpha} \qquad (5)$$

Substituindo (4) e (5) em (1) obtem-se:

$$\frac{MS_i(m)}{\mu_*^2} = \frac{C_i\,\overline{\Phi}_\varepsilon^{2/3}\,(1.5\,\gamma^e)^3\,f^{\gamma^e}}{\left(1+\frac{1.5\,\gamma^e}{(fm)^\alpha}\,f^\alpha\right)^3\,\overline{[(fm)^2]}^B}$$

considerando-se $\gamma^e = 1$, $\alpha = 5/3$ e $B = 1$, chegamos na forma final, dada pela Eq. (4) do artigo

$$\frac{MS_i(m)}{\mu_*^2} = \frac{1.5\,C_i\,\overline{\Phi}_\varepsilon^{2/3}\,f}{\left(1+1.5\,\frac{f^{5/3}}{\overline{[(fm)_i]}^{5/3}}\right)\overline{[(fm)_i]}^{5/3}}$$

5

Vamos calcular a variância da velocidade generalizada

$$S_i(M) = \frac{1.5\, C_i\, \bar{\Phi}_\varepsilon^{2/3}\, Z/U\, \mu_*^2}{\left[(f_M)_i^{5/3} + 1.5 \left(\frac{Z}{U}\right)^{5/3} M^{5/3} \right]}$$

$$\sigma_i^2 = \int_0^\infty S_i(M)\, dM = 1.5\, C_i\, \bar{\Phi}_\varepsilon^{2/3}\, \frac{Z}{U}\, \mu_*^2 \int_0^\infty \frac{dM}{\left[(f_M)_i^{5/3} + 1.5 \left(\frac{Z}{U}\right)^{5/3} M^{5/3} \right]} \quad (6)$$

$$\int_0^\infty \frac{dM}{(f_M)_i^{5/3} + 1.5 \left(\frac{Z}{U}\right)^{5/3} M^{5/3}}$$

$$\int_0^\infty \frac{dx}{a + b\, x^p} \quad (7)$$

no qual $a = (f_M)_i^{5/3}$, $b = 1.5 \left(\frac{Z}{U}\right)^{5/3}$

e $p = 5/3$

Vamos fazer uma mudança de variável

$$x = \left(\frac{a}{b}\right)^{1/p} z \quad \rightarrow \quad x^p = \frac{a}{b} z^p$$

e $$dx = \left(\frac{a}{b}\right)^{1/p} dz$$

Substituindo-se em (7) obtem-se

$$\left(\frac{a}{b}\right)^{1/p} \int_0^\infty \frac{dz}{a + b \frac{a}{b} z^p}$$

$$= \frac{1}{a} \left(\frac{a}{b}\right)^{1/p} \int_0^\infty \frac{dz}{1 + z^p}$$

Do teorema dos resíduos pode-se escrever

$$\int_0^\infty \frac{dz}{1 + z^p} = \frac{\pi}{p \operatorname{sen} \pi/p}$$

então

$$\int_0^\infty \frac{dx}{a+b\,x^p} = \frac{1}{a}\left(\frac{a}{b}\right)^{1/p} \frac{\pi}{p\,\operatorname{sen}\,\pi/p}$$

$$= \frac{1}{(fm)_i^{5/3}} \left[\frac{(fm)_i^{5/3}}{1.5\,(2/v)^{5/3}}\right]^{3/5} \frac{\pi}{\frac{5}{3}\operatorname{sen}\frac{3}{5}\pi} \qquad (7)$$

$$= \frac{1}{(fm)_i^{2/3}} \frac{\pi}{1.5\,(2/v)^{\frac{5}{3}}\operatorname{sen}\frac{3}{5}\pi}$$

Substituindo (7) em (6), finalmente pode-se escrever

$$\sigma_i^2 = \frac{2.32\,c_i\,\Phi_\varepsilon^{2/3}\,\mu_*^2}{(fm)_i^{2/3}}$$

Eq. (7) do artigo

Available online at www.sciencedirect.com
ScienceDirect
Atmospheric Environment 41 (2007) 7059–7068
ATMOSPHERIC ENVIRONMENT
www.elsevier.com/locate/atmosenv

Employing Heisenberg's turbulent spectral transfer theory to parameterize sub-filter scales in LES models

Gervásio A. Degrazia[a,*], André B. Nunes[b], Prakki Satyamurty[b], Otávio C. Acevedo[a], Haroldo F. de Campos Velho[c], Umberto Rizza[d], Jonas C. Carvalho[e]

[a]*Departamento de Física, Universidade Federal de Santa Maria, Santa Maria, RS, Brazil*
[b]*CPTEC, Instituto Nacional de Pesquisas Espaciais, São José dos Campos, SP, Brazil*
[c]*LAC, Instituto Nacional de Pesquisas Espaciais, São José dos Campos, SP, Brazil*
[d]*Istituto di Scienze dellÁtmosfera e del Clima, CNR, Lecce, Italy*
[e]*Faculdade de Meteorologia, Universidade Federal de Pelotas, Pelotas, RS, Brazil*

Received 11 October 2006; received in revised form 23 April 2007; accepted 2 May 2007

Abstract

A turbulent subfilter viscosity for large eddy simulation (LES) models is proposed, based on Heisenberg's mechanism of energy transfer. Such viscosity is described in terms of a cutoff wave number, leading to relationships for the grid mesh spacing, for a convective boundary layer (CBL). The limiting wave number represents a sharp filter separating large and small scales of a turbulent flow and, henceforth, Heisenberg's model agrees with the physical foundation of LES models. The comparison between Heisenberg's turbulent viscosity and the classical ones, based on Smagorinsky's parameterization, shows that both procedures lead to similar subgrid exchange coefficients. With this result, the turbulence resolution length scale and the vertical mesh spacing are expressed only in terms of the longitudinal mesh spacing. Through the employment of spectral observational data in the CBL, the mesh spacings, the filter width and the subfilter eddy viscosity are described in terms of the CBL height. The present development shows that Heisenberg's theory naturally establishes a physical criterium that connects the subgrid terms to the large-scale dimensions of the system. The proposed constrain is tested employing a LES code and the results show that it leads to a good representation of the boundary layer variables, without an excessive refinement of the grid mesh.

Keywords: LES subfilter; Heisenberg model; Convective boundary layer

and e is the turbulent kinetic energy (TKE) of subfilter scales (SFSs). For neutral (zero surface turbulent heat flux) or unstable (positive turbulent surface heat flux) conditions, l_0 is equal to the low-pass LES filter width Δ.

Following Weil et al. (2004), the low-pass LES filter width is given by

$$\Delta = \left[\left(\frac{3}{2} \right)^2 \Delta x \Delta y \Delta z \right]^{1/3}, \tag{3}$$

where Δx, Δy and Δz are the computational mesh sizes in the three coordinate directions x, y, z and the constant $(3/2)^2$ accounts for the dealiasing. Therefore, the filter width Δ is of the order of the numerical grid dimension and the choice of their value may be guided by the typical scales of the CBL flow. In fact, this choice will depend on the available computer power and the range of scales that needs to be actually resolved for the pertinent description of the investigated problem. For a LES resolving the energy-containing eddies in a CBL the filter width Δ can be chosen in the inertial subrange, closer to the integral scale, and far from Kolmogorov's dissipative scale.

Furthermore, the turbulence dissipation rate ε is parameterized as (Moeng, 1984)

$$\varepsilon = c_\varepsilon \frac{e^{3/2}}{l}, \tag{4}$$

where c_ε is a constant (0.93).

3. Heisenberg model for the KTV

In his classical work, based on intuitive arguments, Heisenberg (1948) assumed that the process of the energy transfer from the small to the large wave numbers in a Kolmogorov turbulent spectrum is similar to the conversion of mechanical energy into thermal energy through the agency of molecular viscosity. In other words, the physical picture that forms the basis of Heisenberg's theory is that, in the energy cascade process within the kinetic turbulent spectrum, the mechanism of inertial exchange of energy from large to small eddies is controlled by a KTV. Thus, the effect of the inertia term can be regarded as equivalent to a virtual turbulent friction, ν_T, produced by the small-scale turbulence (inertial subrange eddies), acting on the large-scale turbulence (energy-containing eddies). ν_T represents the KTV, which as a consequence of the lack of correlation between large and small separated Fourier elements of the spectrum (statistical independence between turbulent scales), is a property of the inertial subrange turbulent eddies, whose scales range from an arbitrary but fixed wave number to infinity (since dissipative scales and molecular viscosity are irrelevant, as mentioned before). Therefore, the magnitude of KTV will depend on the inertial subrange eddies that cause the viscosity, and hence must depend on eddies with wave numbers in the range (k_c, ∞), where k_c is a cutoff or limiting wave number for the inertial subrange, which can be determinated from the experimental TKE spectra.

An eddy viscosity is the product of a characteristic turbulent length scale and a velocity, and thus dimensional analysis yields (Heisenberg, 1948—see also Hinze, 1975)

$$\nu_T = \int_{k_c}^{\infty} C_H \sqrt{\frac{E(k)}{k^3}}\, dk, \tag{5}$$

where k is the wave number, C_H is Heisenberg's dimensionless spectral transfer constant and $E(k)$ is the three-dimensional (3-D) turbulence energy spectrum in the inertial subrange, with the following form (Kolmogorov, 1941):

$$E(k) = \alpha_K \varepsilon^{2/3} k^{-5/3}, \tag{6}$$

where α_K is the Kolmogorov constant. Assuming that the small-scale turbulence (inertial subrange) should act on the large-scale turbulence like an additional eddy viscosity we substitute Eq. (6) into Eq. (5), where $C_H \approx 0.47$ and $\alpha_K \approx 1.52$ (Muschinski and Roth, 1993; Corrsin, 1963), to obtain

$$\nu_T = 0.44\varepsilon^{1/3}k_c^{-4/3}. \tag{7}$$

It is important to note that Eq. (7) was firstly derived by Muschinski and Roth (1993).

Following the philosophy of Kraichnan's eddy viscosity in spectral space, Lesieur and Métais (1996) present an eddy viscosity expressed by

$$\nu_T = \frac{2}{3}\alpha_K^{-3/2}\left[\frac{E(k_c)}{k}\right]^{1/2}, \tag{8}$$

where $E(k_c)$ is the kinetic energy spectrum at the cutoff k_c.

Now, substituting Eq. (6) with $k = k_c$ in Eq. (8) yields

$$\nu_T = 0.44\varepsilon^{1/3}k_c^{-4/3} \tag{9}$$

suggesting that Heisenberg's eddy viscosity is identical to the one proposed by Lesieur and Métais

Contents lists available at SciVerse ScienceDirect

Physica A

journal homepage: www.elsevier.com/locate/physa

Employing Taylor and Heisenberg subfilter viscosities to simulate turbulent statistics in LES models

G.A. Degrazia [a,*], U. Rizza [b], F.S. Puhales [a], G.S. Welter [a], O.C. Acevedo [a], S. Maldaner [a]

[a] Laboratório de Física da Atmosfera, UFSM, Santa Maria, RS, Brazil

[b] Istituto di Science dell'Atmosfera e del Clima, Consiglio Nazionale delle Ricerche, Lecce, Italy

ARTICLE INFO

Article history:
Received 16 September 2011
Available online 5 October 2011

Keywords:
Large-eddy simulation
Subfilter models
Convective boundary layer

ABSTRACT

A turbulent subfilter viscosity for Large Eddy Simulation (LES) based on the Taylor statistical diffusion theory is proposed. This viscosity is described in terms of a velocity variance and a time scale, both associated to the inertial subrange. This new subfilter viscosity contains a cutoff wavenumber k_c, presenting an identical form (differing by a constant) to the Heisenberg subfilter viscosity. Therefore, both subfilter viscosities are described in terms of a sharp division between large and small wavenumbers of a turbulent flow and, henceforth, Taylor and Heisenberg subfilter viscosities are in agreement with the sharp Fourier filtering operation, frequently employed in LES models. Turbulent statistics of different orders, generated from atmospheric boundary layer simulations employing both Taylor and Heisenberg subfilter viscosities have been compared with observations and results provided by other simulations. The comparison shows that the LES model utilizing the approaches of Taylor and Heisenberg reproduces these turbulent statistics correctly in different vertical regions of a planetary convective boundary layer (CBL).

1. Introduction

The planetary boundary layer (PBL) is a physical system presenting a variety of complex states characterized by the turbulence phenomenon. An understanding of the turbulence patterns and its structural details is of fundamental importance in large and small meteorological scales and atmospheric dispersion. From the numerical point of view, the PBL turbulence has been investigated employing Large-Eddy Simulation (LES) models [1–7]. In LES, only the energy-containing eddies of the degrees of freedom of the turbulent field are explicitly resolved and the effect of the smaller, more isotropic eddies (typically those in the inertial subrange), needs to be parameterized [8]. Modeling these residual turbulent motions, also termed subfilter-scale (SFS) motions [9], is in large part a phenomenological procedure based on heuristic arguments [10]. The basic equations in the LES models are the incompressible Navier–Stokes equations described for a horizontally homogeneous boundary layer. The resolved turbulent flow time-dependent random variables are determined by the application of a low-pass spatial filter presenting a characteristic width, known as the turbulent resolution length scale [9]. It is smaller than the scales of the resolved turbulent motions. The filter scale is within or at least close to an inertial subrange of the turbulent energy spectrum [11]. According to [12], "the parameterization of the residual stress term in the large-eddy equation is dynamically essential; it causes the transference of kinetic energy to smaller scales. Thus, its parameterization is a key step in developing a large eddy model".

Considering a fully developed turbulence as a state with a quasi infinite number of degrees of freedom (myriads of excited energy modes), the parameterization of residual stress means to reproduce the physical effects of a large number of higher frequency harmonics (subfilter scales), which, by virtue of the filtering operation are not explicitly resolved in a numerical simulation.

Most residual stress term models employ a subfilter turbulent viscosity [4]. The concept of subfilter viscosity is based on the fact that the energy transfer mechanism from the resolved to the subfilter scales is similar to the molecular mechanism represented by a viscosity.

A widely employed parameterization for the residual stress tensor is described by [13,10,4]

$$\tau_{ij} = -\nu_T \left(\frac{\partial u_i}{\partial x_j} + \frac{\partial u_j}{\partial x_i} \right) \tag{1}$$

where u_i and u_j are the resolved velocity components, and $i, j = 1, 2, 3$ corresponding to the (x, y, z) cartesian directions respectively and ν_T is the subfilter turbulent viscosity proposed by Refs. [1,14], which is expressed as

$$\nu_T = c_k \ell_0 \sqrt{e} \tag{2}$$

where $c_k = 0.1$ is a constant, ℓ_0 is a mixing-length scale related to the filter operation [11] and e is the turbulent kinetic energy of the subfilter scales (SFS). More recent applications of LES have almost exclusively employed a subfilter turbulent viscosity [15]. Recently, based on the Heisenberg turbulent spectral energy transfer theory, [16] proposed a subfilter eddy viscosity for LES models that has been expressed in terms of the cutoff or limiting wave number for the inertial subrange.

The purpose of the present study is to derive a new turbulent subfilter eddy viscosity based on the energy at cutoff from the Taylor statistical diffusion theory and compare it with the Heisenberg subfilter viscosity. This comparison is accomplished by introducing both subfilter models in the LES code of Moeng and Sullivan [2,10] to investigate distinct turbulent characteristics of a CBL.

2. Heisenberg and Taylor subfilter turbulent viscosities

The starting point of the derivation consists in considering the structure of the 3D turbulent spectrum in geophysical flows, such as the PBL, where Reynolds numbers are very large (infinite Reynolds number limit). In such situations, the turbulent energy spectra can be subdivided in three major spectral regions: energy-containing, inertial and dissipation subranges [17]. In the energy-containing subrange, the large eddies provide the main contribution to the turbulent kinetic energy and the density spectrum shows its maximum. It is possible, therefore, to choose its corresponding frequency n_e that characterizes the evolution time of the most energetic eddies. In the dissipation subrange, where the molecular viscosity ν plays its major role, it is also possible to associate a frequency n_d with the timescales that provide the main contribution to the dissipation. Therefore, for fully developed turbulence, the dissipation in frequencies far below that of maximum dissipation will be negligibly small compared with the energy flux by inertial effects. In such an inertial subrange, the effect of molecular viscosity would then vanish, so that $\nu_T \gg \nu$. As a consequence we may associate a frequency n_c, such that n_c is a cutoff or limiting frequency for the inertial subrange, with the scale of the eddies that provide the main contribution to inertial energy flux, so that

$$n_e \ll n_c \ll n_d. \tag{3}$$

With this assumption $n_e \ll n_c$, the inertial subrange turbulence is statistically independent of the energy-containing eddies and a relationship for the subfilter turbulent viscosity ν_T can be obtained. Thus, following the Taylor statistical diffusion theory, which represents for short and long time limit an eddy diffusivity expressed as the product of a velocity variance by a time [15], a subfilter turbulent viscosity can be obtained from the following general formulation

$$\nu_T = \sigma_l^2 T_c \tag{4}$$

where T_c is the Lagrangian time scale associated to the frequency n_c given by [18]

$$T_c = \frac{1}{6}\frac{\beta}{n_c}. \tag{5}$$

In Eq. (5), β is defined as the ratio of the Lagrangian to the Eulerian time scales and σ_l^2 is the turbulent velocity variance for the inertial subrange [19] have shown rigorously that for an isotropic turbulence $\beta = (\sqrt{\pi}/4)/(u/\sigma_l)$, resulting

$$\nu_T = \frac{\sqrt{\pi}}{24}\frac{u\sigma_l}{n_c} \tag{6}$$

where u is the mean wind speed. Substituting $k_c = 2\pi n_c/u$, where k_c is the cutoff or limiting wave number for the inertial subrange, into Eq. (6) yields

$$\nu_T = \frac{\pi^{3/2}}{12}\frac{\sigma_l}{k_c}. \tag{7}$$

Considering Kolmogorov's turbulent energy spectrum in the inertial subrange, represented by Ref. [20]

$$E(k) = \alpha_k \varepsilon^{3/2} k^{-5/3} \tag{8}$$

where ε is the turbulent dissipation rate and $\alpha_k = 1.4$ is the Kolmogorov constant [21], an expression for σ_l is given by the relation

$$\sigma_l = (3\alpha_k)^{1/2} \left(\frac{\varepsilon}{k_c} \right)^{1/3}. \tag{9}$$

Finally, employing (9) in Eq. (7), results

$$\nu_T = 0.95 \varepsilon^{1/3} k_c^{-4/3} \tag{10}$$

suggesting that the Taylor subfilter turbulent viscosity, as given by (10), presents an identical functional form (differing by a constant) to the one derived firstly by Ref. [22], from the Heisenberg turbulent spectral energy transfer theory and expressed as Ref. [16]

$$\nu_T = 0.44 \varepsilon^{1/3} k_c^{-4/3}. \tag{11}$$

Subfilter eddy viscosity as given by Eq. (11) is identical to the spectral eddy diffusivity proposed by Ref. [4]. the Taylor subfilter viscosity given by Eq. (10) presents a numerical coefficient that is larger by a factor greater than 100%.

Subfilter viscosity models represented by formulations (10) and (11) are classified as models based on the energy at cutoff. According to Ref. [21], the relevance for these models lies on the fact that "*the information is contained in the resolved field, but localized in frequency and therefore theoretically more pertinent for describing the phenomena at cutoff than quantities that are global and thus not localized in frequency. Such models ensure that the subgrid viscosity will be null if the flow is well resolved, i.e. if the highest frequency mode captured by the grid is zero. This type of model thus ensure a better physical consistency than those models based on large scales*". the Taylor and Heisenberg theory (Eqs. (10) and (11)) establish that the energy transfer from smaller wavenumbers than a given value to larger can be represented as the effect of a turbulent viscosity. This introduces a separation between scales at any arbitrary wavenumber in the inertial subrange. This scale division is indeed naturally relevant in the LES methodology, where a cutoff wavenumber is arbitrarily chosen in the inertial subrange introducing then an artificial sharp division (connected with the sharp Fourier cutoff filter), to which the Taylor and Heisenberg approach seem well suited to be applied.

Furthermore, the presence of the cutoff wavenumber in Eqs. (10) and (11) allows the selection of filter widths that ensure the condition $k_c \gg k_p$ in proximity to the ground (such criterion guarantees that the resolved turbulent motions are dominant, where k_p is the peak wavenumber of the turbulent energy spectrum [23], Eq. (4); [24], Eq. (3)). Therefore, the Taylor and Heisenberg parameterization can be employed to obtain a kinematic eddy viscosity, which represents the effects of the inertial subrange filtered eddies.

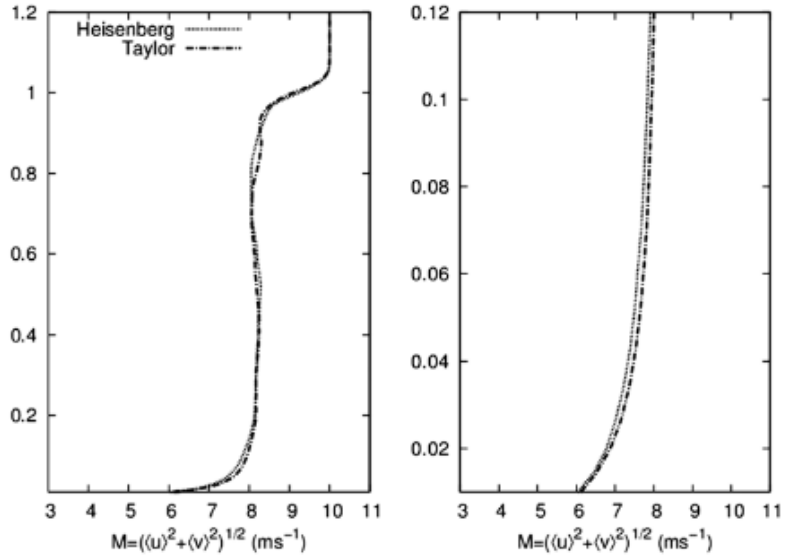

Fig. 1. Average wind speed vertical profile $M = (\langle U \rangle^2 + \langle V \rangle^2)^{1/2}$. $\langle U \rangle$ and $\langle V \rangle$ are, respectively, the x and y components of the mean wind speed.

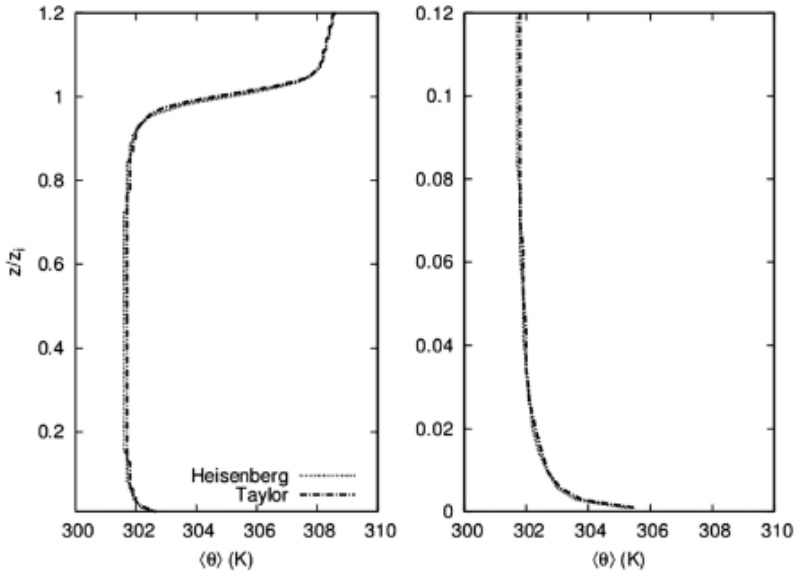

Fig. 2. Average potential temperature vertical profile.

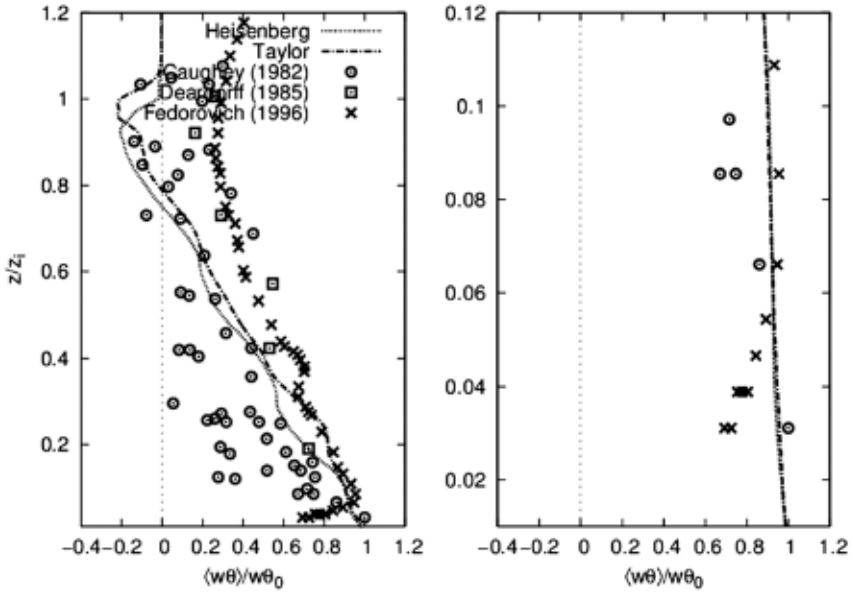

Fig. 6. Vertical profile of the normalized heat flux.

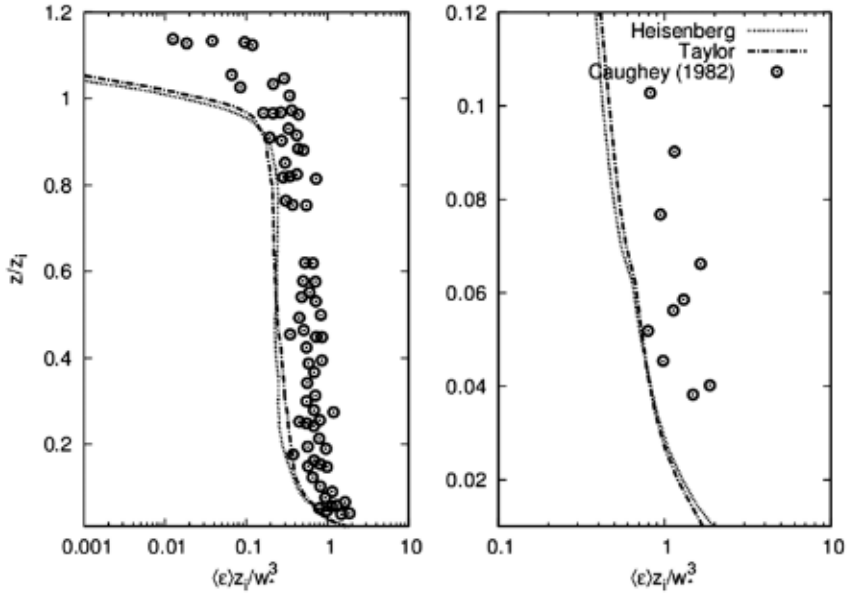

Fig. 7. Vertical profile of the dissipation rate.

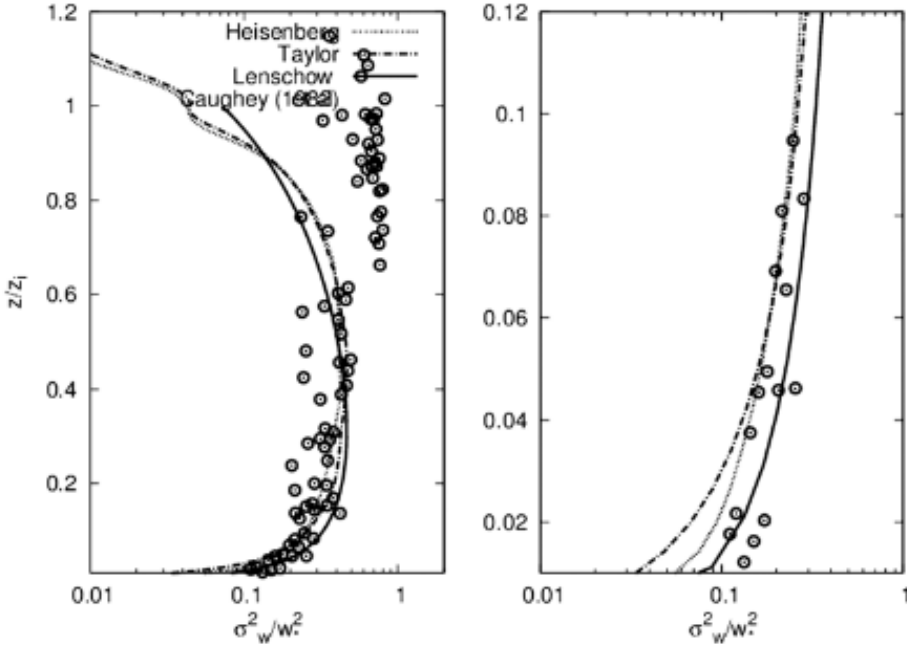

Fig. 8. Vertical profile of the normalized vertical velocity variance.

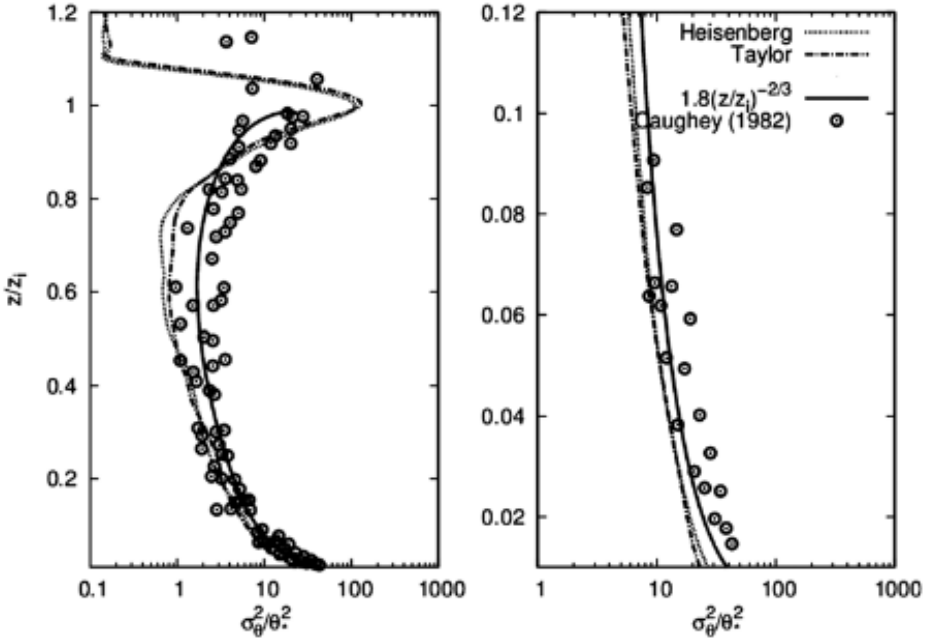

Fig. 10. Vertical profile of the normalized temperature variance.

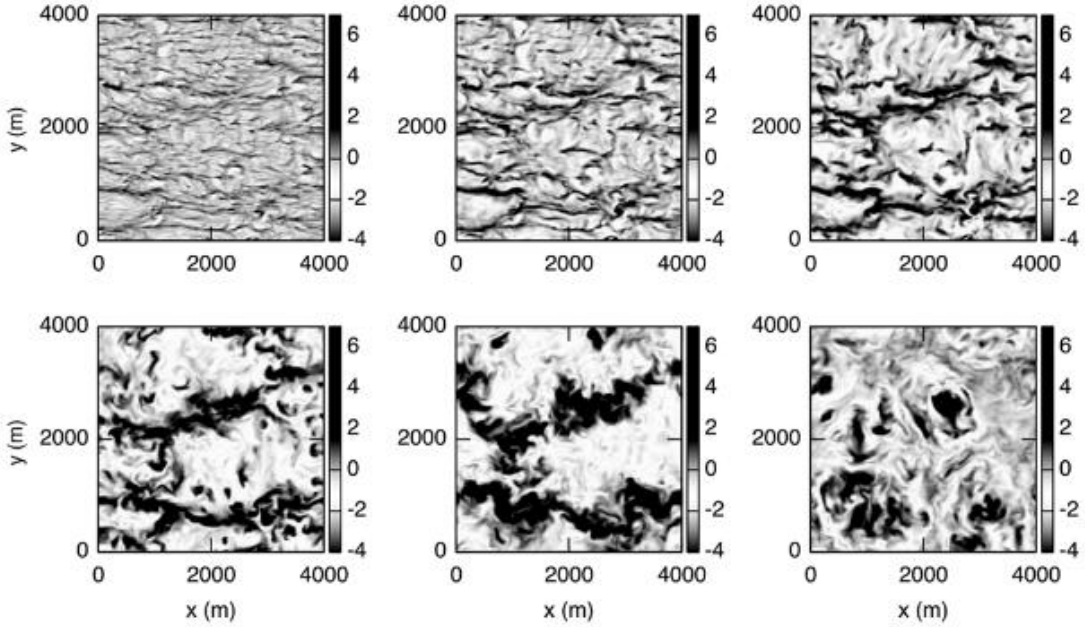

Fig. 12. Contours of the vertical velocity on horizontal planes at different heights.

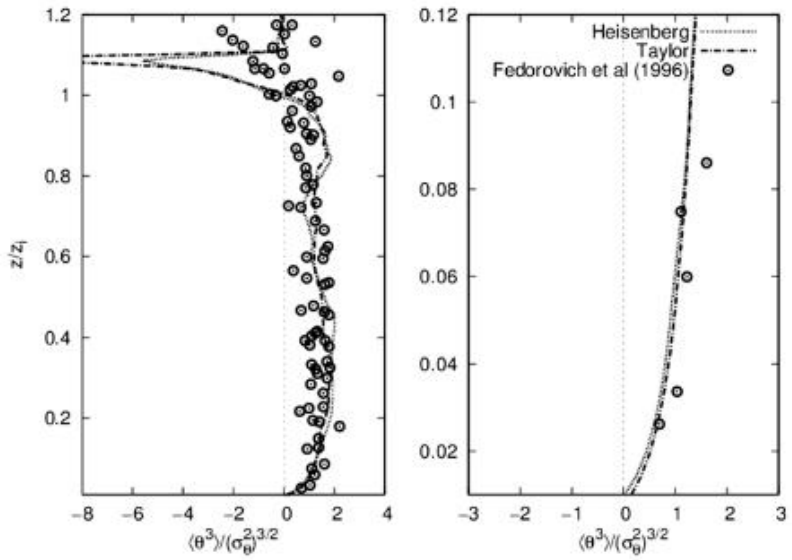

Fig. 13. Vertical profile of the temperature skewness.

Contents lists available at ScienceDirect

Physica A

journal homepage: www.elsevier.com/locate/physa

Proposal of a new autocorrelation function in low wind speed conditions

L.P. Moor [a,b,*], G.A. Degrazia [c], M.B. Stefanello [c], L. Mortarini [d], O.C. Acevedo [c], S. Maldaner [e], C.R.P. Szinvelski [f], D.R. Roberti [c], L. Buligon [f], D. Anfossi [d]

[a] Programa de Pós-Graduação em Física, UFSM, Santa Maria, RS, Brazil
[b] Coordenação Geral de Ensino, IF Farroupilha, Jaguari, RS, Brazil
[c] Departamento de Física, UFSM, Santa Maria, RS, Brazil
[d] Institute of Atmospheric Sciences and Climate (ISAC) of the Italian National Research Council (CNR), Unit of Turin, Italy
[e] Coordenadoria Acadêmica, UFSM -campus Cachoeira do Sul, RS, Brazil
[f] Departamento de Matemática, UFSM, Santa Maria, RS, Brazil

HIGHLIGHTS

- We propose a new mathematical expression to describe the meandering phenomenon.
- We employ wind data measured in a nocturnal PBL to obtain experimental ACF.
- The new ACF satisfactorily represents the negative lobes of the meandering phenomenon.

ARTICLE INFO

Article history:
Received 27 June 2015
Available online 9 July 2015

Keywords:
Meandering
Autocorrelation function
Low wind speed
Fit curves

ABSTRACT

In this study a new mathematical expression to describe the observed meandering autocorrelation functions in low-wind speed is proposed. The analysis utilizes a large number of best fit curves to show that the proposed theoretical function well reproduces the general form and the negative lobes characterizing the experimental meandering autocorrelation function. Further, the good agreement of the measured autocorrelation curves with the proposed algebraic autocorrelation function allows to calculate the magnitudes of the meandering period and of the loop parameter. The results agree with the values presented and discussed in the literature. Therefore, the new formulation describing experimental meandering autocorrelation functions can be used to simulate the dispersion of contaminant during low wind episodes and to determine relevant meandering parameters.

1. Introduction

The autocorrelation function (ACF) is a statistical quantity relevant both for dispersion studies and to obtain fundamental equations associated to the turbulence phenomenon. In this aspect, the employment of autocorrelation functions obtained from experimental data for different movement patterns in the planetary boundary layer (PBL) allows to estimate important

parameters employed to understand complex phenomena in geophysical flows. Simulating turbulent transport and, as a consequence, atmospheric passive scalar diffusion in low wind speed conditions is a difficult physical problem. For very low wind speed conditions, below a certain critical value of the mean wind velocity (about 1–2 m s^{-1}), it is no longer possible to determine a precise mean wind direction since low-frequency horizontal wind oscillations prevail and the dispersion of contaminant in the planetary boundary layer is dominated by these degrees of freedom that disperse the contaminant plume over a rather wide angular sector [1,2]. In the literature, these large horizontal wind oscillations are called meandering and are responsible for the fact that the observed autocorrelation functions of the horizontal wind velocity components show a looping behavior, characterized by the presence of negative lobes [1–4]. Normally, classical functions such as the exponential function [5], which adequately describes fully developed turbulence, fail completely to describe the observed meandering autocorrelation functions [1]. Anfossi et al. [1] proposed to utilize the well known Frenkiel's form [6] to fit the meandering ACF determined in low wind-speed.

The aim of this study is to present a new autocorrelation function, alternative to the Frenkiel's form to describe the observed negative lobes in the meandering of the horizontal mean wind vector. The new function (Eq. (3)) is a hybrid expression constituted by both turbulent and meandering characteristic parameters describing pure and connected states of turbulent and meandering movements. In Section 2, the new proposed ACF is presented. In Section 3 it is tested on meandering observations measured at a pasture site in the Brazilian Amazon region [7]. An additional purpose is to employ this new autocorrelation function, with the dataset measured in Brazilian Amazon region to evaluate the meandering time scale and the loop parameter magnitudes in nocturnal and stable low wind speed cases. The mean values of the meandering period and of the loop parameter are then used to determine the magnitudes of the turbulent integral time scale. Additionally, values of the meandering period are related to the mean wind speed. All these topics are presented and discussed in Section 4.

2. Obtaining the meandering autocorrelation function

For a fully developed turbulence, the autocorrelation function for the horizontal wind velocity components u, v may be written as [8]

$$R_{u,v}(\tau) = \left(1 + \frac{\tau}{T_{u,v}}\right)^{-2} \tag{1}$$

where τ is the time lag and $T_{u,v}$ is the turbulent integral time scale, defined by the following relationship

$$T_{u,v} = \int_0^\infty R_{u,v}(\tau)\, d\tau. \tag{2}$$

This integral time scale describes the memory effect associated to the organized eddies patterns that compose a turbulent flow. Eq. (1) well describes the scalars lateral turbulent dispersion in the situation of high wind speeds in the PBL. On the other hand, for very low wind conditions, when the observed autocorrelation function presents negative lobes [1,4], Eq. (1) fails to describe the scalars dispersion in the PBL. Therefore, considering these manifold manifestations, characterized by cases in which turbulence coexists with low-frequency motion associated to the meandering phenomenon, the following new formulation is suggested:

$$R_{u,v}(\tau) = \cos\left(\frac{m_{u,v}\tau}{(m_{u,v}^2+1)T_{u,v}}\right) \Big/ \left(1 + \frac{\tau}{(m_{u,v}^2+1)T_{u,v}}\right)^2. \tag{3}$$

Eq. (3) is a hybrid expression containing $T_{u,v}$ and the loop parameter $m_{u,v}$, that controls the meandering oscillation frequency associated to the horizontal wind. High values of $m_{u,v}$ characterize a strong manifestation of the meandering (accentuated negative lobes) [9]. Differently, very low magnitudes of $m_{u,v}$ are associated to fully developed turbulence. Such behavior can be seen in Fig. 1, where Eq. (3) is plotted for different values of the loop parameter. This figure shows the presence of negatives lobes associated to the meandering movement, whose relevance is enhanced as $m_{u,v}$ increases.

It is worth noticing that for $m_{u,v}$ approaching zero Eq. (3) tends to Eq. (1). Eq. (3) can also be written in a different manner, namely

$$R_{u,v}(\tau) = \frac{\cos(q_{u,v}\tau)}{(1 + p_{u,v}\tau)^2} \tag{4}$$

with

$$p_{u,v} = \frac{1}{(m_{u,v}^2 + 1)T_{u,v}} \tag{5}$$

and

$$q_{u,v} = \frac{m_{u,v}}{(m_{u,v}^2 + 1)T_{u,v}} \tag{6}$$

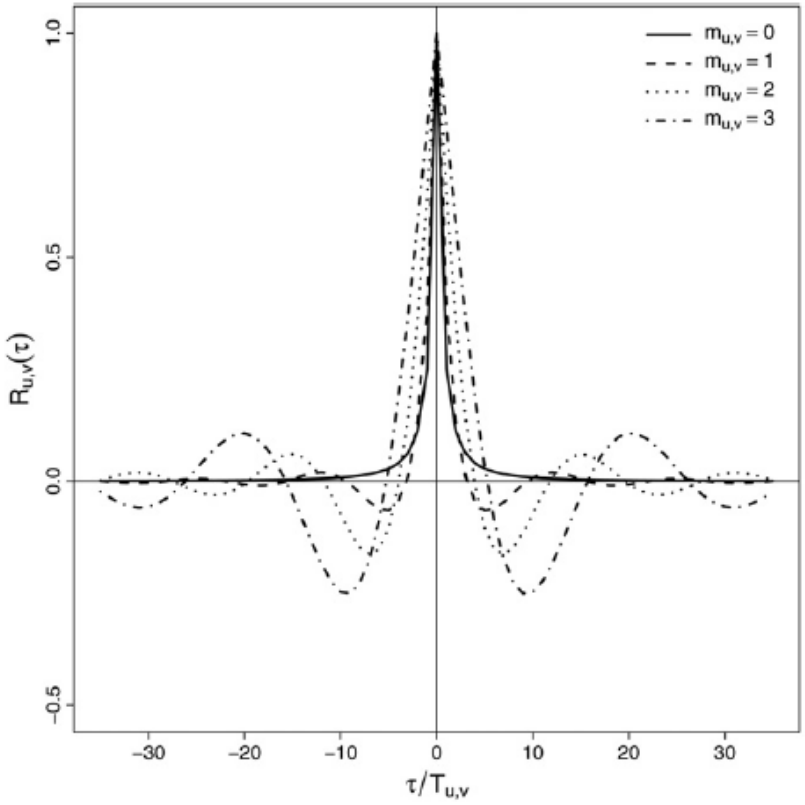

Fig. 1. Autocorrelation functions obtained from Eq. (3) using different values of the loop parameter.

$p_{u,v}$ and $q_{u,v}$ are hybrid quantities described in terms of $T_{u,v}$ and $m_{u,v}$. It is important to note that from Eqs. (5) and (6) a meandering time scale (meandering period) can be defined as $T_{*_{u,v}} = 2\pi/q_{u,v}$ and will be expressed by [1]

$$T_{*_{u,v}} = \frac{2\pi T_{u,v}(m_{u,v}^2 + 1)}{m_{u,v}}. \tag{7}$$

Such meandering period is a fundamental parameter to provide air quality precise forecasting [4,10]. Analyzing Eq. (7) for large values of $m_{u,v}$, the following equation yields:

$$m_{u,v} \approx \frac{1}{2\pi}\frac{T_{*_{u,v}}}{T_{u,v}}. \tag{8}$$

Defining $m_{u,v}$ as the ratio of meandering period to the turbulent integral time scale.

3. Fitting observed meandering ACF with Eq. (3)

In this section, we employ meandering data measured in a nocturnal stable low wind speed PBL to obtain experimental autocorrelation functions. These experimental functions are fitted with the new meandering autocorrelation function (Eq. (3)). Thus, Eq. (3) is validated as a mathematical formulation to describe the observed negative lobes in the meandering autocorrelation functions and employed to provide the loop parameter ($m_{u,v}$) and the meandering period ($T_{*_{u,v}}$). The meandering data were collected in a Brazilian Amazon Large Scale Biosphere–Atmosphere project (LBA dataset; [7]). The wind velocities components were sampled at a frequency of 10 Hz by a sonic anemometer (SATI/3K Applied Technologies, Inc., Longmont, CO, USA) located at one level of 8.75 m in a flat pasture region (3.0121° latitude S; 54.5371° longitude W). The dataset employed in this study were continuously measured between January and September 2003.

Figs. 2–5 show characteristic results of the comparison among the ACFs calculated on the LBA low wind speed dataset (gray line) and the associated best fit (black line) evaluated from the new ACF (Eq. (3)). All figures were obtained from one hour nocturnal time series having the mean horizontal speed less than 1.5 m s^{-1}. This limit wind speed value is in agreement with the magnitudes of the low wind speed suggested by Anfossi et al. [1] and Mortarini et al. [11] for the existence of the meandering phenomenon. It can be seen that for these graphs the ACF minimum values, associated to the negative lobes, characterizing the horizontal wind meandering range from −0.61 to −0.53.

From the analysis of 1474 best fit curves of low wind meandering ACF, we can conclude that Eq. (3) provides a good or fairly good fit in about 80% of the observed meandering events. Thus, the present analysis shows that the proposed function, given by Eq. (3), adequately represents the observed form of the meandering ACF. Particularly, its oscillatory behavior and the large negative lobes characterizing the wind meandering phenomenon.

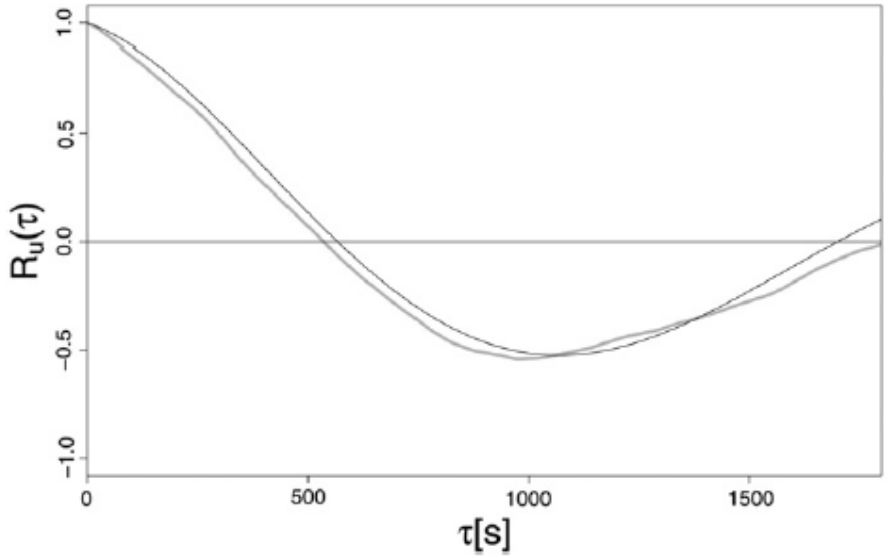

Fig. 2. Comparison between the ACF calculated on the LBA low wind speed dataset (gray line) and the associated best fit (black line) evaluated from Eq. (3). For January 08, 0100 local time, $\overline{U} = 0.47$ m s^{-1}.

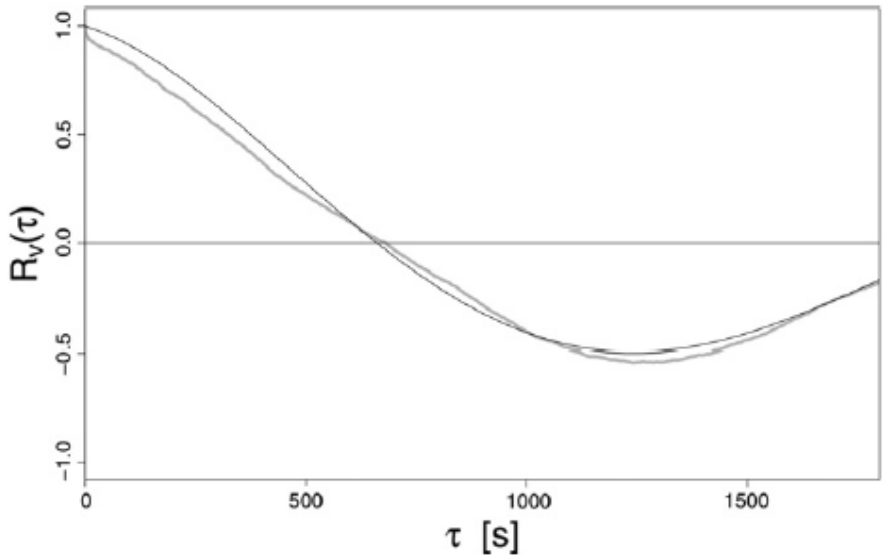

Fig. 3. As in Fig. 2, for January 08, 2100 local time, $\overline{U} = 0.11$ m s^{-1}.

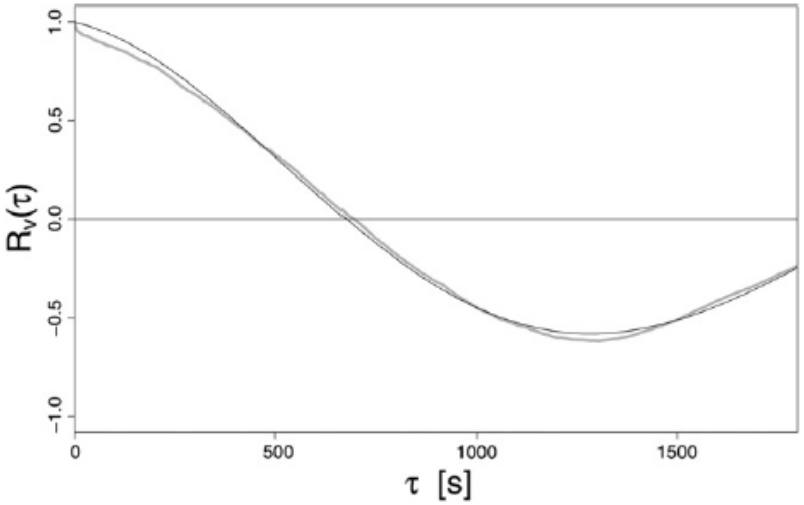

Fig. 5. As in Fig. 2, for January 13, 0300 local time, $\overline{U} = 0.94$ m s^{-1}.

Table 1
Meandering period and loop parameter average values for the u and v components.

	T_{*_u} (s)	T_{*_v} (s)	m_u	m_v
Amazon dataset	2202	2204	4.8	5.1

Table 1 shows these mean values for the wind u and v velocity components averaged over 1474 (mean wind speed less than 1.5 m s^{-1}) observed meandering events. It can be seen that the m_u and m_v values as well as the T_{*_u} and T_{*_v} values are very similar to each other. These magnitudes for T_{*_u} and T_{*_v} agree very well with the mean value found by Anfossi et al. [1] employing the best fit for the meandering ACF determined from the Frenkiel's form [6]. The magnitudes of m_u and m_v in Table 1 are sufficiently large confirming the approximation described by Eq. (8). Therefore, the substitution of the values of $T_{*_{u,v}}$ and $m_{u,v}$ into Eq. (8) provides the following mean values for the integral time scales, $T_u \approx 73$ s and $T_v \approx 69$ s.

Degrazia et al. [13] derived the following formulation to calculate the integral time scales $T_{u,v}$ for a nocturnal stable boundary layer (NBL)

$$T_{u,v} = \frac{z}{\sqrt{c_{u,v}}} \left\{ \frac{0.50}{u_* \phi_\varepsilon^{1/3} \left(1 + 3.7 \frac{z}{L(1-z/h)^{5/4}}\right)^{2/3}} \right\} \tag{9}$$

with the non-dimensional turbulence dissipation rate ϕ_ε given by [14]

$$\phi_\varepsilon = 1.1 \left(1 + 3.7 \frac{z}{L(1-z/h)^{5/4}}\right) \tag{10}$$

where $z = 8.75$ m is the anemometer height above the surface, $c_{u,v}$ are, respectively, 0.27 and 0.36 (turbulence isotropy condition), u_* is the friction velocity, L is the Obukhov length and h is the NBL depth. Considering the 1474 meandering cases analyzed in this study, we determine the following mean values for the friction velocity ($u_* = 0.095$ m s^{-1}) and Obukhov length ($L = 141$ m). Acevedo et al. [15] modeling the NBL in the Amazon pasture region suggested for the NBL depth (h) a value of the order of 100 m. The substitution of these values into Eqs. (9) and (10) yields $T_u = 70$ s and $T_v = 60$ s. These results are close to the values of $T_u \approx 73$ s and $T_v \approx 69$ s previously found using Eq. (8).

Fig. 6 exhibits the dependence of the meandering period on the mean wind speed for the whole LBA dataset (2222 h). The points represent average on wind speed classes. These best fit curves represent the whole set of the observed mean wind speeds. From this figure, it can be seen that, as expected, the magnitude of the meandering characteristic time scale decreases with velocity. The analysis also shows that the largest values of the meandering period occur when the mean wind speed is less than 1.5 m s^{-1}.

Fig. 7, obtained from the 2222 best fit curves, presents the joint dependence of the analyzed wind data distribution on the mean wind speed and on the meandering period for u component. This figure confirms the information provided by Fig. 6. Furthermore, it shows in a visible way that an elevated number of cases for mean wind speed less than 1 m s^{-1} is associated to high values of the meandering period. It can be seen also from this figure that for low wind cases the meandering period varies between 1500 s and 3000 s. These values for the meandering period are in agreement with studies accomplished by Anfossi et al. [1] and Mortarini et al. [11].

The good results and agreements discussed and obtained in this study ensure that the mathematical formulation given by Eq. (3) can be used to investigate the distinct properties of the meandering phenomenon in the PBL.

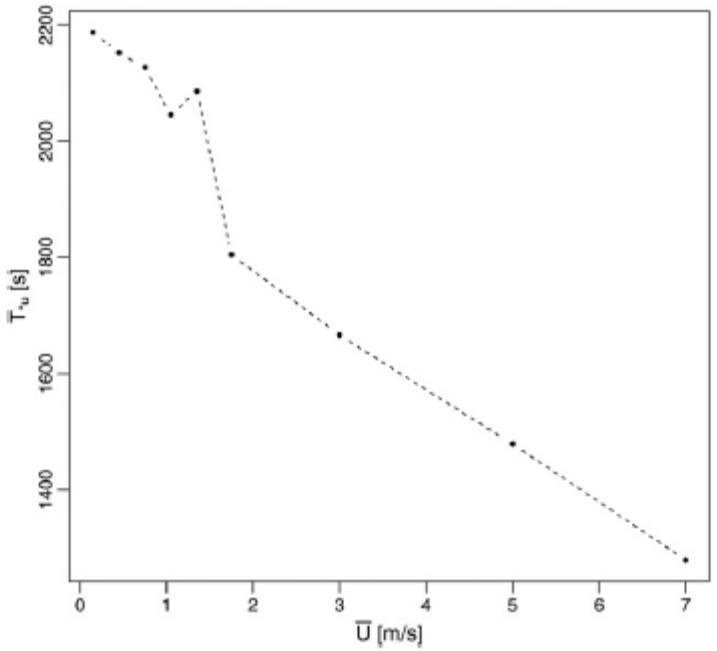

Fig. 6. Relation between the mean wind speed magnitude and the period of meandering (u component).

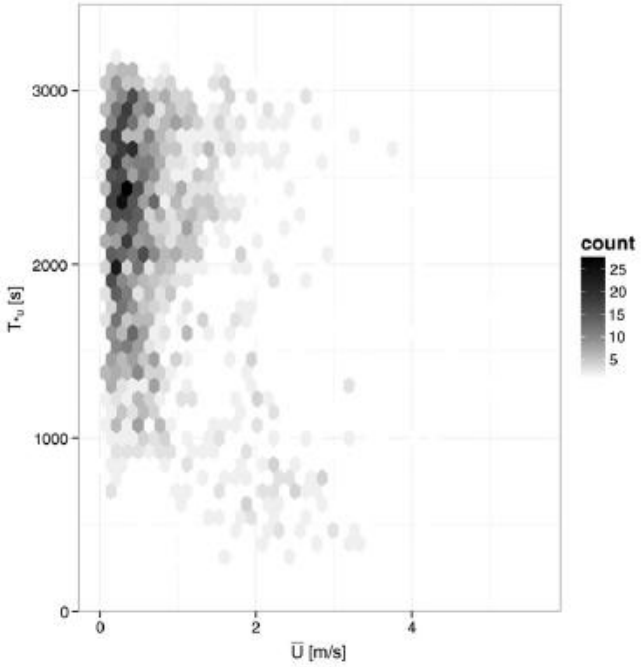

Fig. 7. Wind data distribution with the wind mean speed and the meandering period (u component).

Boundary-Layer Meteorol
DOI 10.1007/s10546-016-0165-6

RESEARCH ARTICLE

Characterization of Wind Meandering in Low-Wind-Speed Conditions

Luca Mortarini[1] · Michel Stefanello[2] · Gervasio Degrazia[2] · Debora Roberti[2] · Silvia Trini Castelli[1] · Domenico Anfossi[1]

Received: 7 September 2015 / Accepted: 26 April 2016

Abstract Investigation of low-wind cases observed during the Urban Turbulent Project campaign (Torino, Italy) and at the Santa Maria meteorological station (Santa Maria, Brazil) provides insight into the wind-meandering phenomenon, i.e. large, non-turbulent oscillations of horizontal wind speed and temperature. Meandering and non-meandering cases are identified through analysis of the Eulerian autocorrelation functions of the horizontal wind-velocity components and temperature. When all three autocorrelation functions oscillate, meandering is present. As with weak turbulence, meandering shows no dependence on stability but is influenced by presence of buildings and depends on wind speed. We show that, while the standard deviation of the horizontal velocity is always large in low-wind conditions, the standard deviation of the vertical velocity shows very different behaviour in meandering and non-meandering conditions. In particular, the value of the ratio of the standard deviations of the vertical and horizontal velocities typifies the meandering condition.

Quarterly Journal of the Royal Meteorological Society *Q. J. R. Meteorol. Soc.* (2016) DOI:10.1002/qj.2796

RMetS
Royal Meteorological Society

Temperature auto-correlation and spectra functions in low-wind meandering conditions

L. Mortarini,[a*] S. Maldaner,[b] L. P. Moor,[c,d] M. B. Stefanello,[e] O. Acevedo,[e] G. Degrazia[e] and D. Anfossi[a]

[a]*Institute of Atmospheric Sciences and Climate, National Research Council, Torino, Italy*
[b]*Universidade Federal de Santa Maria - Campus de Cachoeira do Sul, Santa Maria, Brazil*
[c]*Programa de Pós-Graduação em Física, Universidade Federal de Santa Maria, Santa Maria, Brazil*
[d]*Coordenação Geral de Ensino, Instituto Federal de Educação, Ciência e Tecnologia Farroupilha - Câmpus Jaguari, Santa Maria, Brazil*
[e]*Curso de Física, Universidade Federal de Santa Maria, Santa Maria, Brazil*

*Correspondence to: L. Mortarini. Corso Fiume 4, 10133 Torino, Italia. E-mail: l.mortarini@isac.cnr.it

Eulerian low-wind temperature statistics are investigated through the analysis of sonic anemometer observations gathered in two experimental campaigns, the Urban Turbulent Project in Northern Italy and the Large-Scale Biosphere-Atmosphere Experiment in Amazonia (Brazil). The observed auto-correlations and spectra functions are tested with the theoretical relationships previously proposed for the horizontal velocity components in low wind speed conditions. The comparison showed that the temperature field, similarly to the horizontal velocity field, presents a characteristic oscillatory behaviour with a distinct isolated spectrum peak frequency due to the wind meandering. The ratio between this frequency and the one associated to the horizontal velocity components is close to one. This, together with the similarity between the temperature and velocity spectra and auto-correlation functions, suggests that a dynamical link between temperature and velocity oscillations exists.

Employing the Hilbert-Huang Transform to analyse observed natural complex signals: calm wind meandering cases

Luis Gustavo Nogueira Martins[1], Michel Baptistella Stefanello[1], Gervásio Annes Degrazia[1], Otávio Costa Acevedo[1], Franciano Scremin Puhales[1], Giuliano Demarco[1], Luca Mortarini[2], Domenico Anfossi[2], Débora Regina Roberti[1], Felipe Costa Denardin[3], Silvana Maldaner[1]

Abstract

In this study we analyze natural complex signals employing the Hilbert-Huang spectral analysis. Specifically, low wind meandering meteorological data are decomposed in turbulent and non turbulent components. These non turbulent movements, responsible by the absence of a preferential direction of the horizontal wind, provoke negative lobes in the meandering autocorrelation functions. The meandering characteristic time scales (meandering periods) are determined from the spectral peak provided by the Hilbert-Huang marginal spectrum. The magnitudes of the temperature and horizontal wind meandering period obtained agree with the results found from the best fit of the heuristic meandering autocorrelation functions. Therefore, the new method represents a new procedure to evaluate meandering periods that does not employs mathematical expressions to represent observed meandering autocorrelation functions.

questions?

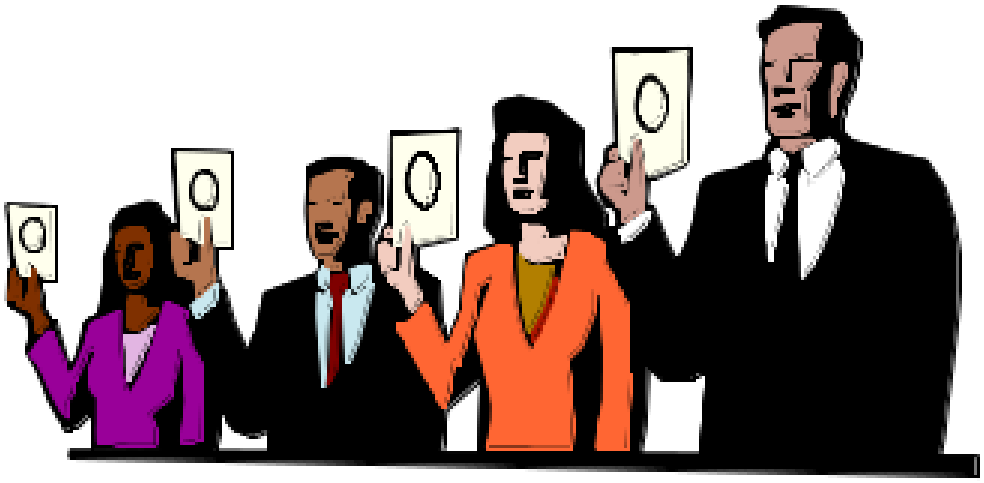

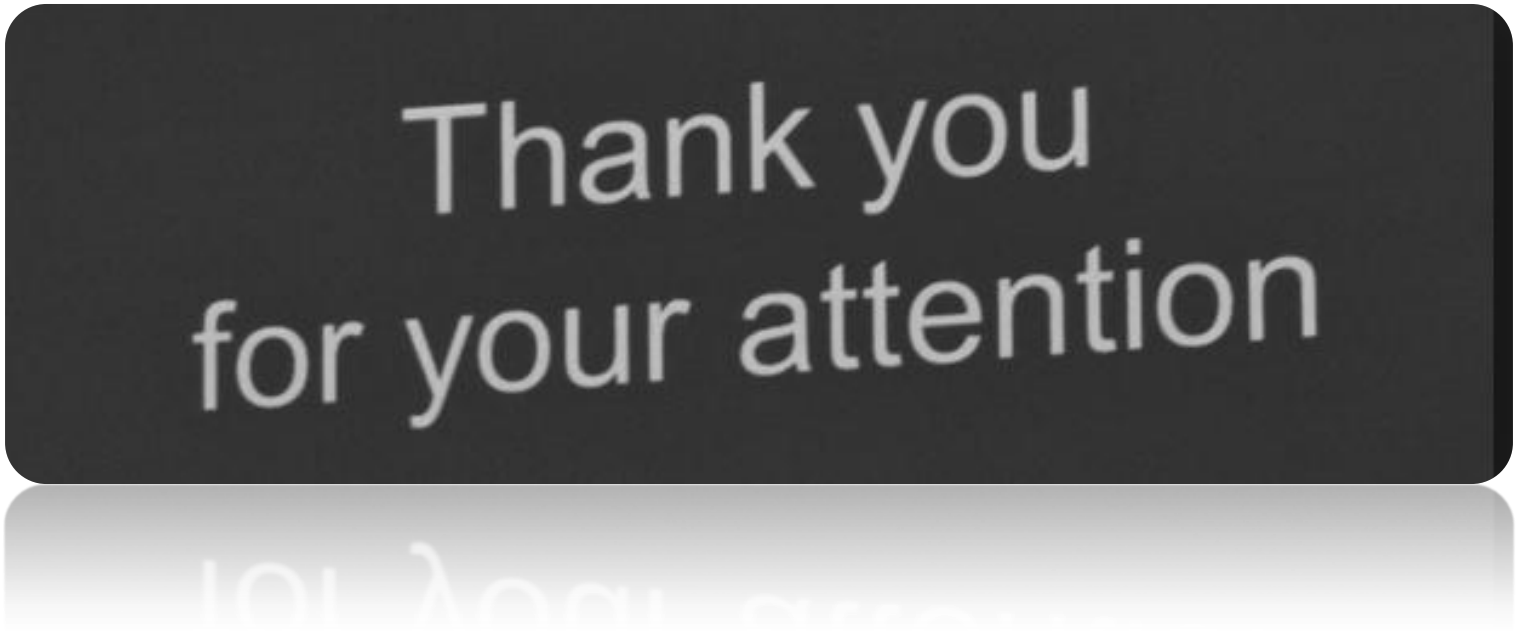
Thank you
for your attention